A Finite Element Approach to Modelling Fractal Ultrasonic Transducers

Ebrahem A. Algehyne and Anthony J. Mulholland

Department of Mathematics and Statistics

University of Strathclyde

Livingstone Tower, 26 Richmond Street

Glasgow, UK

G1 1XH

December 10, 2013

Abstract

Piezoelectric ultrasonic transducers usually employ composite structures to improve their transmission and reception sensitivities. The geometry of the composite is regular with one dominant length scale and, since these are resonant devices, this dictates the central operating frequency of the device. In order to construct a wide bandwith device it would seem natural therefore to utilize resonators that span a range of length scales. In this article we derive a mathematical model to predict the dynamics of a fractal ultrasound transducer; the fractal in this case being the Sierpinski gasket. Expressions for the electrical and mechanical fields that

are contained within this structure are expressed in terms of a finite element basis. The propagation of an ultrasonic wave in this transducer is then analyzed and used to derive expressions for the non-dimensionalised electrical impedance and the transmission and reception sensitivities as a function of the driving frequency. Comparing these key performance measures to an equivalent standard (Euclidean) design shows some benefits of these fractal designs.

1 Introduction

Ultrasonic transducers are devices that convert electrical energy into mechanical vibration and conversely can convert mechanical energy into an electrical signal [21]. These devices can be used to interrogate a medium by emitting a wave (electrical to mechanical) and then listening to the same wave after it has traversed the medium (mechanical to electrical). Piezoelectric ultrasonic transducers typically employ composite structures to improve their transmission and reception sensitivities [9, 18]. Many biological species produce and receive ultrasound such as moths, bats, dolphins and cockroaches. The manmade transducers tend to have very regular geometry on a single scale whereas the natural systems exhibit a wide variety of intricate geometries often with resonators over a range of length scales [16, 15, 13, 4, 6, 17, 19, 5]. This allows these transducers to operate over a wider frequency range and hence results in reception and transmission sensitivities with exceptional bandwidths. To assess the benefits of having transducers with such structures it would be useful to build mathematical models of them. One structure whose geometrical components consist of a range of length scales is a fractal. There have been a number of mathematical

approaches which describe wave propagation in fractal media [11, 8, 12, 1, 2]. This paper constructs a model of a fractal ultrasound transducer and then uses this model to compare its operational qualities with that of a standard (Euclidean) design. The fractal that will be used in this article to simulate this self-similar transducer is the Sierpinski gasket [7]. Such an ultrasonic transducer would start with an equilateral triangle of piezoelectric crystal, and the next generation ($n = 1$) would be obtained by replacing this by three copies of itself, each of which being half the size of the original triangle. This process is then repeated for several generations (see Figure 1). The Sierpinski gasket lattice of degree 3, SG(3), is the lattice counterpart of the Sierpinski gasket [20] (see Figure 2). This lattice is constructed by a process which starts from the Sierpinski gasket of order 1 (which consists of three piezoelectric triangles), assigns a vertex to the centre of each of these triangles and, by connecting these vertices together with edges, the SG(3) lattice at generation level $n = 1$ is constructed. The lattice has side length L units which remains constant as the generation level n increases. Therefore, as n increases, the length of the edge between adjacent vertices tends to zero and in this limit the lattice will perfectly match the space filling properties of the original Sierpinski gasket [14]. The total number of vertices is $N = 3^n$ and $h^{(n)} = L/(2^n - 1)$ is the edge length of the fractal lattice. The vertex degree is 3 apart from the boundary vertices (input/output vertices) which have degree 2 and $M = 2(3^n - 1)/3$ denotes the total number of edges. These boundary vertices will be used to interact with external loads (both electrical and mechanical) and so we introduce fictitious vertices A, B and C to accommodate these interfacial boundary conditions (see Figures 5 and 6). Let us denote by Ω the set of points lying on the edges or vertices of $SG(3)$ and denote the region's boundary by $\partial\Omega$.

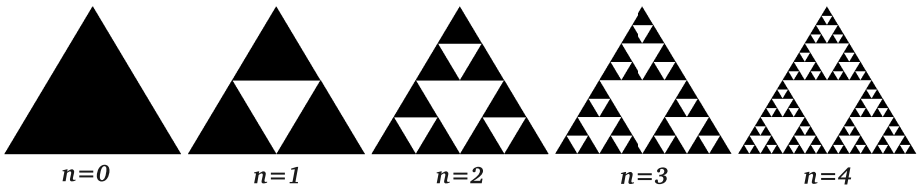

Figure 1: The first few generations of the Sierpinski gasket.

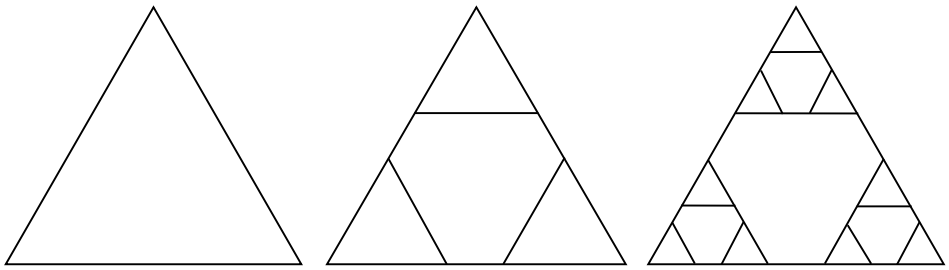

Figure 2: The first few generations of the Sierpinski gasket lattice $SG(3)$.

2 Model Derivation

The lattice represents the vibrations of a piezoelectric material (we will focus on PZT-5H) that has been manufactured to form a Sierpinski gasket. The interplay between the electrical and mechanical behaviour of the lattice vertices is therefore described by the piezoelectric constitutive equations [21]

$$T_{ij} = c_{ijkl}S_{kl} - e_{kij}E_k, \tag{1}$$

$$D_i = e_{ikl}S_{kl} + \varepsilon_{ik}E_k, \tag{2}$$

where T_{ij} is the stress tensor, c_{ijkl} is the stiffness tensor, S_{kl} is the strain tensor, e_{kij} is the piezoelectric tensor, D_i is the electrical displacement tensor and ε_{ik} is the permittivity tensor (where the Einstein summation convention is adopted). The strain tensor is related to the displacement gradients $u_{i,j}$ by

$$S_{ij} = \frac{u_{i,j} + u_{j,i}}{2}, \tag{3}$$

and the electric field vector is related to the electric potential ϕ via

$$E_i = -\phi_{,i}. \tag{4}$$

The dynamics of the piezoelectric material is then governed by

$$\rho_T \ddot{u}_i = T_{ji,j}, \tag{5}$$

subject to Gauss' law

$$D_{i,i} = 0 \tag{6}$$

where ρ_T is the density and u_i is the component of displacement in the direction of the i^{th} basis vector. So, combining equations (5) and (1) gives

$$\rho_T \ddot{u}_i = c_{jikl} S_{kl,j} - e_{kji} E_{k,j}. \tag{7}$$

Combining equations (6) and (2)

$$D_{i,i} = e_{ikl} S_{kl,i} + \varepsilon_{ik} E_{k,i} = 0. \tag{8}$$

We will restrict attention to the out of plane displacement only (a horizontal shear wave) by stipulating that

$$\underline{u} = \big(0, 0, u_3(x_1, x_2, t)\big), \tag{9}$$

so only $u_{3,1}$ and $u_{3,2}$ are nonzero then equation (7) gives

$$\rho_T \ddot{u}_3 = c_{13kl} S_{kl,1} + c_{23kl} S_{kl,2} - e_{kj3} E_{k,j}. \tag{10}$$

From equation (3) we get

$$S_{ij} = \begin{cases} \frac{1}{2} u_{3,1} & i = 1, j = 3 \text{ or } i = 3, j = 1 \\ \frac{1}{2} u_{3,2} & i = 2, j = 3 \text{ or } i = 3, j = 2 \\ 0 & \text{otherwise,} \end{cases} \tag{11}$$

so equation (10) gives

$$\rho_T \ddot{u}_3 = c_{1331}u_{3,11} + c_{1332}u_{3,21} + c_{2331}u_{3,12} + c_{2332}u_{3,22} - e_{kj3}E_{k,j}. \tag{12}$$

From the properties of PZT-5H (see Appendix), then

$$\rho_T \ddot{u}_3 = c_{44}(u_{3,11} + u_{3,22}) - e_{kj3}E_{k,j}. \tag{13}$$

since $c_{55} = c_{44}$. Now if $\underline{E} = \big(E_1(x_1, x_2), E_2(x_1, x_2), 0\big)$ then

$$\rho_T \ddot{u}_3 = c_{44}(u_{3,11} + u_{3,22}) - e_{113}E_{1,1} - e_{123}E_{1,2} - e_{213}E_{2,1} - e_{223}E_{2,2}. \tag{14}$$

That is

$$\rho_T \ddot{u}_3 = c_{44}(u_{3,11} + u_{3,22}) - e_{15}E_{1,1} - e_{14}E_{1,2} - e_{25}E_{2,1} - e_{24}E_{2,2}. \tag{15}$$

Then, for PZT-5H,

$$\rho_T \ddot{u}_3 = c_{44}(u_{3,11} + u_{3,22}) - e_{24}(E_{1,1} + E_{2,2}), \tag{16}$$

since $e_{15} = e_{24}$. From equation (8) we get

$$e_{113}S_{13,1} + e_{131}S_{31,1} + e_{223}S_{23,2} + e_{232}S_{32,2} + \varepsilon_{11}E_{1,1} + \varepsilon_{22}E_{2,2} = 0. \tag{17}$$

That is, for PZT-5H,

$$e_{15}u_{3,11} + e_{24}u_{3,22} + \varepsilon_{11}E_{1,1} + \varepsilon_{22}E_{2,2} = 0. \tag{18}$$

Therefore

$$e_{24}(u_{3,11} + u_{3,22}) + \varepsilon_{11}(E_{1,1} + E_{2,2}) = 0 \tag{19}$$

since $\varepsilon_{11} = \varepsilon_{22}$. So we get

$$E_{1,1} + E_{2,2} = -\frac{e_{24}}{\varepsilon_{11}}(u_{3,11} + u_{3,22}). \tag{20}$$

Substituting this equation into equation (16) gives

$$\rho_T \ddot{u}_3 = c_{44}(u_{3,11} + u_{3,22}) + \frac{e_{24}^2}{\varepsilon_{11}}(u_{3,11} + u_{3,22}). \tag{21}$$

This can be written as

$$\ddot{u}_3 = c_T^2 \nabla u_3 \tag{22}$$

where $\nabla = (\partial^2/\partial x_1^2, \partial^2/\partial x_2^2)$, $c_T = \sqrt{Y_T/\rho_T}$ is the (piezoelectrically stiffened) wave velocity and $Y_T = c_{44}(1 + e_{24}^2/(\varepsilon_{11}c_{44}))$. We impose the initial conditions $u_3(\underline{x}, 0) = \dot{u}_3(\underline{x}, 0) = 0$ and the boundary conditions of continuity of displacement and force at $\partial\Omega$ (the boundary to Ω). By introducing the non-dimensionalised variable $\theta = c_T t/h$ then (dropping the subscript on u)

$$\frac{\partial^2 u}{\partial \theta^2} = h^2 \nabla^2 u. \tag{23}$$

Applying the Laplace transform $\mathcal{L} : \theta \to q$ then gives

$$q^2\ \bar{u} = h^2\ \nabla^2 \bar{u}. \tag{24}$$

We will seek a weak solution $\bar{u} \in H^1(\Omega)$ where on the boundary $\bar{u} = \bar{u}_{\partial\Omega} \in H^1(\partial\Omega)$. Now multiplying by a test function $w \in H_B^1(\Omega)$, where $H_B^1(\Omega) := \{w \in H^1(\Omega) : w = 0 \,\text{on}\, \partial\Omega\}$, integrating over the region Ω, and using Green's first identity $\int_\Omega \psi\ \nabla^2\phi\, dv = \oint_{\partial\Omega} \psi(\nabla\phi.\underline{n})\, dr - \int_\Omega \nabla\phi.\nabla\psi\, dv$, where $\underline{n}$ is the outward pointing unit normal of surface element dr, gives

$$\int_\Omega q^2\ \bar{u}\ w\, d\underline{x} = h^2 \oint_{\partial\Omega} w(\nabla\bar{u}.\underline{n})\, dr - h^2 \int_\Omega \nabla\bar{u}.\nabla w\, d\underline{x}. \tag{25}$$

Now $h^2 \oint_{\partial\Omega} w(\nabla\bar{u}.\underline{n})\, dr$ is zero since $w = 0$ on $\partial\Omega$ and so, we seek $\bar{u} \in H^1(\Omega)$ such that

$$\int_\Omega (q^2\ \bar{u}\ w + h^2\ \nabla\bar{u}.\nabla w)\, d\underline{x} = 0 \tag{26}$$

where $w \in H_B^1(\Omega)$.

3 Galerkin discretisation

Using a standard Galerkin method we replace $H^1(\Omega)$ and $H^1_B(\Omega)$ by the finite dimensional subspaces S and $S_B = S \cap H^1_B(\Omega)$. Let $U_B \in S$ be a function that approximates $\bar{u}_{\partial\Omega}$ on $\partial\Omega$, then the discretised problem involves finding $\bar{U} \in S$ such that

$$\int_\Omega (q^2\ \bar{U}\ W + h^2\ \nabla\bar{U}.\nabla W)\, d\underline{x} = 0. \tag{27}$$

Let$\{\phi_1, \phi_2, \cdots, \phi_N\}$ form a basis of S_D and set $W = \phi_j$, then

$$\int_\Omega (q^2\ \bar{U}\ \phi_j + h^2\ \nabla\bar{U}.\nabla\phi_j)\, d\underline{x} = 0. \tag{28}$$

Furthermore, let $I = \{\phi_{N+1}, \phi_{N+2}, \phi_{N+3}\}$ form a basis for the boundary nodes and let

$$\bar{U} = \sum_{i=1}^{N} U_i\phi_i + \sum_{i\in I} U_{B_i}\phi_i. \tag{29}$$

Hence, equation (28) becomes

$$\begin{aligned}\sum_{i=1}^{N}\left(\int_\Omega (q^2\phi_i\phi_j + h^2\nabla\phi_i.\nabla\phi_j)d\underline{x}\right)U_i = \\ -\sum_{i\in I}\left(\int_\Omega (q^2\phi_i\phi_j + h^2\nabla\phi_i.\nabla\phi_j)d\underline{x}\right)U_{B_i}\end{aligned} \tag{30}$$

where $j \in \{1, 2, \cdots, N\}$. That is

$$A_{ji}U_i = b_j \tag{31}$$

where

$$A_{ji} = \int_\Omega (q^2\phi_i\phi_j + h^2\nabla\phi_i.\nabla\phi_j)d\underline{x}, \tag{32}$$

and

$$b_j = -\sum_{i\in I}\left(\int_\Omega (q^2\phi_i\phi_j + h^2\nabla\phi_i.\nabla\phi_j)d\underline{x}\right)U_{B_i}. \tag{33}$$

It is important to now explicitly record the fractal generation level n and so equation (32) can be written

$$A_{ji}^{(n)} = q^2\, H_{ji}^{(n)} + h^2\, K_{ji}^{(n)}, \tag{34}$$

where

$$K_{ji}^{(n)} = \int_{\Omega} (\nabla\phi_j . \nabla\phi_i) d\underline{x} \tag{35}$$

and

$$H_{ji}^{(n)} = \int_{\Omega} (\phi_j \phi_i) d\underline{x}. \tag{36}$$

The lattice basis function at vertex $\underline{x}_j$ is chosen to be (see Figure 3)

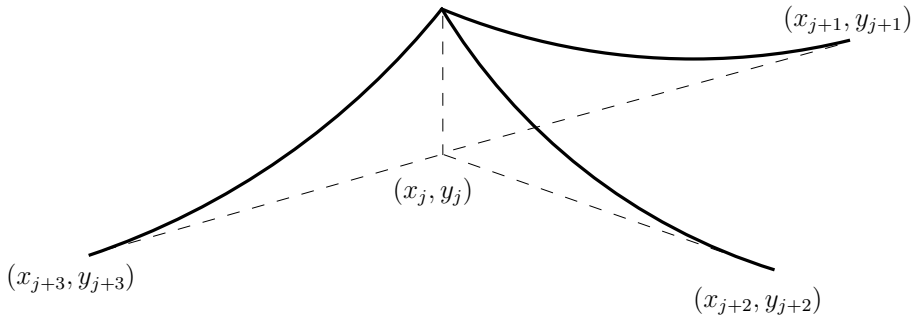

Figure 3: The lattice basis function ϕ_j at vertex $\underline{x}_j = (x_j, y_j)$.

$$\phi_j(x,y) = \begin{cases} a + bx + cy + d(x^2+y^2) & j \in \{1, \cdots, N\} \\ a + d(x^2+y^2) & j \in I. \end{cases} \tag{37}$$

where $(x, y) \in \Omega$ and $a, b, c, d \in \mathbb{R}$ are coefficients to be determined. Hence

$$\nabla\phi_j(x,y) = \begin{cases} (b + 2dx, c + 2dy) & j \in \{1, \cdots, N\} \\ (2dx, 2dy) & j \in I. \end{cases} \tag{38}$$

Futhermore, the ϕ_j are defined as localised basis functions such that

$$\phi_j(x,y) = \begin{cases} 1 & \text{if } (x,y) = (x_j, y_j) \\ 0 & \text{if } (x,y) = \text{coordinates of vertices adjacent to vertex } j, \end{cases} \tag{39}$$

and $\phi_j(x,y) = 0$ at all points which do not lie in the edges adjacent to vertex j. For each generation level of the $SG(3)$ lattice the coordinates of the vertices are known (see the Appendix for a detailed description for $n = 1$ and $n = 2$). Using equation (39) the coefficients in equation (37) can be determined (see the Appendix for the values of these coefficients for $n = 1$ and $n = 2$). For each element (edge) e where $e = 1, \cdots, M$

$$\begin{aligned} {}^eK_{ji}^{(n)} &= \int_e (b_j + 2d_j x, c_j + 2d_j y).(b_i + 2d_i x, c_i + 2d_i y) d\underline{x}, \\ &= \int_e \Big(b_i b_j + 2(d_j b_i + d_i b_j)x + 4d_i d_j x^2 + c_i c_j + 2(d_i c_j + d_j c_i)y \\ &\quad + 4d_i d_j y^2 \Big) d\underline{x}. \end{aligned} \tag{40}$$

For a particular element lying between vertex i and vertex j the isoparametric

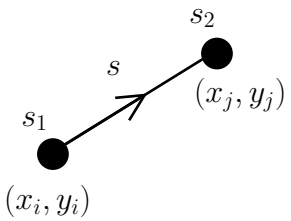

Figure 4: An isoparametric element (edge) between vertex (x_i, y_i) and vertex (x_j, y_j).

representation, given by

$$\Big(x(s), y(s) \Big) = \Big((x_j - x_i)s + x_i, (y_j - y_i)s + y_i \Big) \tag{41}$$

is enployed (see Figure 4), where $s_1 = 0$ and $s_2 = 1$ and $d\underline{x} = hds$. Substituting this into equation (40) gives

$${}^eK_{ji}^{(n)} = \frac{4}{h} \begin{bmatrix} \int_0^1 s^2 ds & \int_0^1 s(s-1) ds \\ \int_0^1 s(s-1) ds & \int_0^1 (s-1)^2 ds \end{bmatrix} = \frac{2}{3h} \begin{bmatrix} 2 & -1 \\ -1 & 2 \end{bmatrix}. \tag{42}$$

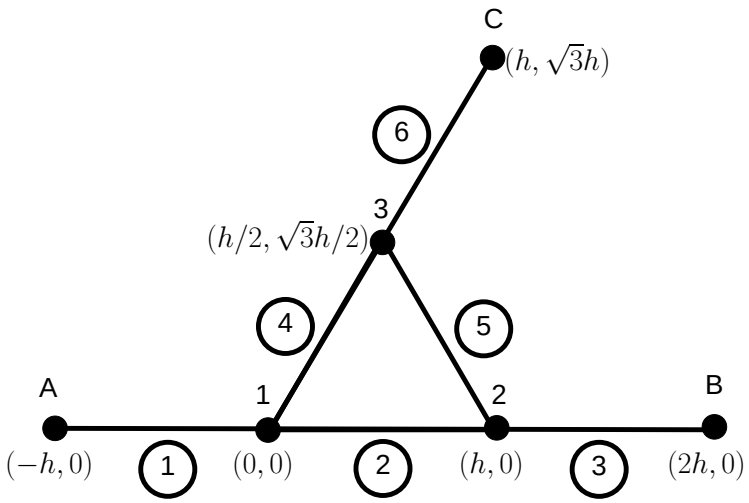

Figure 5: The Sierpinski Gasket lattice $SG(3)$ at generation level $n = 1$. Nodes $1, 2$ and 3 are the input/output nodes, and nodes A, B and C are fictitious nodes used to accommodate the boundary conditions. The lattice has 6 elements (circled numbers), with two vertices adjacent to each element.

For the boundary elements $e \in \{M+1, M+2, M+3\}$ then equation (40) becomes

$$ {}^{e}K_{ji}^{(n)} = \int_{e} (2d_j x, 2d_j y).(2d_i x, 2d_i y) d\underline{x} = \frac{2}{3h} \begin{bmatrix} 2 & 0 \\ 0 & 0 \end{bmatrix}. \tag{43} $$

Combining equations (42) and (43) to assemble the full matrix in equation (35) gives, for generation level $n = 1$,

$$ K_{ji}^{(1)} = \frac{2}{3h} \begin{bmatrix} 6 & -1 & -1 \\ -1 & 6 & -1 \\ -1 & -1 & 6 \end{bmatrix}, \tag{44} $$

and at generation level $n = 2$

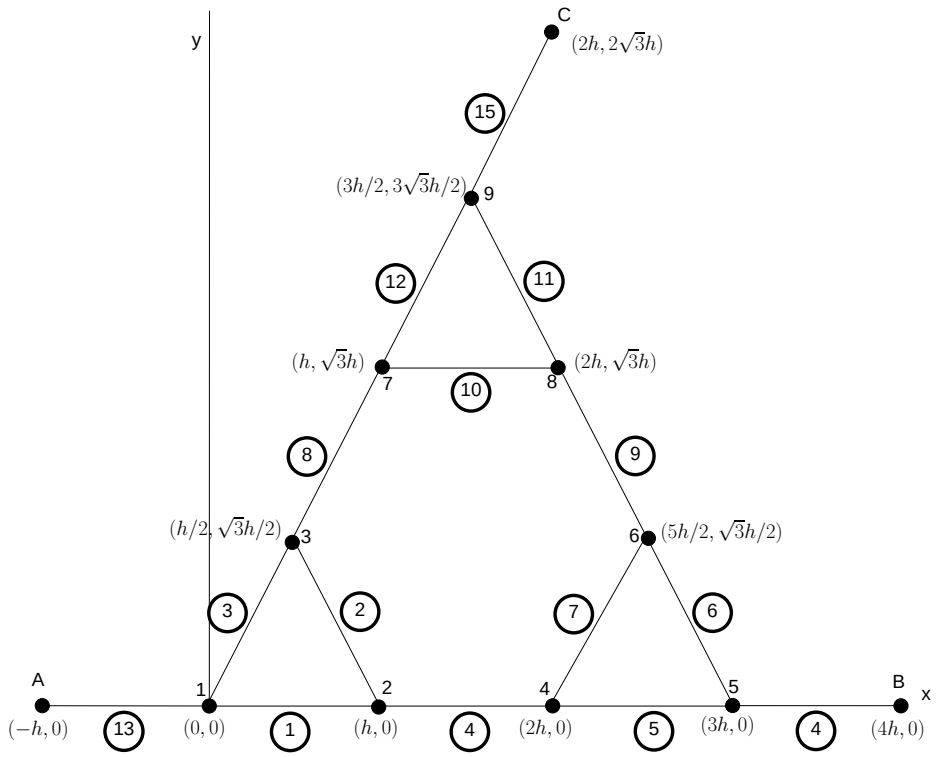

Figure 6: The Sierpinski Gasket lattice $SG(3)$ at generation level $n = 2$. Nodes A, B and C are fictitious nodes used to accommodate the boundary conditions. The lattice has 15 elements (circled numbers), with two vertices adjacent to each element.

$$K_{ji}^{(2)} = \frac{2}{3h} \begin{bmatrix} 6 & -1 & -1 & 0 & 0 & 0 & 0 & 0 & 0 \\ -1 & 6 & -1 & -1 & 0 & 0 & 0 & 0 & 0 \\ -1 & -1 & 6 & 0 & 0 & 0 & -1 & 0 & 0 \\ 0 & -1 & 0 & 6 & -1 & -1 & 0 & 0 & 0 \\ 0 & 0 & 0 & -1 & 6 & -1 & 0 & 0 & 0 \\ 0 & 0 & 0 & -1 & -1 & 6 & 0 & -1 & 0 \\ 0 & 0 & -1 & 0 & 0 & 0 & 6 & -1 & -1 \\ 0 & 0 & 0 & 0 & 0 & -1 & -1 & 6 & -1 \\ 0 & 0 & 0 & 0 & 0 & 0 & -1 & -1 & 6 \end{bmatrix}. \tag{45}$$

Similarly for ${}^{e}H_{ji}^{(n)}$ we can write equation (36) as

$$\begin{aligned}
{}^{e}H_{ji}^{(n)} &= \int_{e} \Big(a_j + b_j x + c_j y + d_j(x^2+y^2).(a_i + b_i x + c_i y + d_i(x^2+y^2)\Big) d\underline{x} \\
&= \int_{e} \Big(a_j a_i + (a_j b_i + a_i b_j)x + (a_j c_i + a_i c_j)y + (c_j b_i + c_i b_j)xy + b_j b_i x^2 \\
&\quad + c_j c_i y^2 + (a_j d_i + a_i d_j)(x^2+y^2) + (b_j d_i + b_i d_j)x(x^2+y^2) \\
&\quad + (c_j d_i + c_i d_j)y(x^2+y^2) + d_j d_i (x^2+y^2)^2\Big) ds^{(e)}. \qquad (46)
\end{aligned}$$

Using equation (41) then

$${}^{e}H_{ji}^{(n)} = h \begin{bmatrix} \int_0^1 (s^2-1)^2 ds & \int_0^1 (s^2-1)(s-2)s ds \\ \int_0^1 (s^2-1)(s-2)s ds & \int_0^1 (s-2)^2 s^2 ds \end{bmatrix}, \qquad (47)$$

for $e \in \{1, \cdots, M\}$ which reduces to

$${}^{e}H_{ji}^{(n)} = \frac{h}{30} \begin{bmatrix} 16 & 11 \\ 11 & 16 \end{bmatrix}. \qquad (48)$$

For the boundary elements $e \in \{M+1, M+2, M+3\}$

$${}^{e}H_{ji}^{(n)} = \frac{h}{30} \begin{bmatrix} 16 & 0 \\ 0 & 0 \end{bmatrix}. \qquad (49)$$

Assembling the full matrix in equation (36) gives, for generation level $n = 1$

$$H_{ji}^{(1)} = \frac{h}{30} \begin{bmatrix} 48 & 11 & 11 \\ 11 & 48 & 11 \\ 11 & 11 & 48 \end{bmatrix}, \qquad (50)$$

and for generation level $n = 2$

$$H_{ji}^{(2)} = \frac{h}{30}\begin{bmatrix} 48 & 11 & 11 & 0 & 0 & 0 & 0 & 0 & 0 \\ 11 & 48 & 11 & 11 & 0 & 0 & 0 & 0 & 0 \\ 11 & 11 & 48 & 0 & 0 & 0 & 11 & 0 & 0 \\ 0 & 11 & 0 & 48 & 11 & 11 & 0 & 0 & 0 \\ 0 & 0 & 0 & 11 & 48 & 11 & 0 & 0 & 0 \\ 0 & 0 & 0 & 11 & 11 & 48 & 0 & 11 & 0 \\ 0 & 0 & 11 & 0 & 0 & 0 & 48 & 11 & 11 \\ 0 & 0 & 0 & 0 & 0 & 11 & 11 & 48 & 11 \\ 0 & 0 & 0 & 0 & 0 & 0 & 11 & 11 & 48 \end{bmatrix}. \tag{51}$$

Combining equations (44) and (50) gives equation (34) as

$$A_{ji}^{(1)} = h\begin{bmatrix} \alpha & \beta & \beta \\ \beta & \alpha & \beta \\ \beta & \beta & \alpha \end{bmatrix}, \tag{52}$$

where $\alpha = \frac{8}{5}q^2 + 4$, and $\beta = \frac{11}{30}q^2 - \frac{2}{3}$. Similarly, for generation level $n = 2$,

$$A_{ji}^{(2)} = h\begin{bmatrix} \alpha & \beta & \beta & 0 & 0 & 0 & 0 & 0 & 0 \\ \beta & \alpha & \beta & \beta & 0 & 0 & 0 & 0 & 0 \\ \beta & \beta & \alpha & 0 & 0 & 0 & \beta & 0 & 0 \\ 0 & \beta & 0 & \alpha & \beta & \beta & 0 & 0 & 0 \\ 0 & 0 & 0 & \beta & \alpha & \beta & 0 & 0 & 0 \\ 0 & 0 & 0 & \beta & \beta & \alpha & 0 & \beta & 0 \\ 0 & 0 & \beta & 0 & 0 & 0 & \alpha & \beta & \beta \\ 0 & 0 & 0 & 0 & 0 & \beta & \beta & \alpha & \beta \\ 0 & 0 & 0 & 0 & 0 & 0 & \beta & \beta & \alpha \end{bmatrix}. \tag{53}$$

A similar treatment can be given to equation (33) to give ($m = (N+1)/2$)

$$b_j^{(n)} = \begin{cases} -(\int_{e_{M+1}} (q^2 \phi_{N+1}\phi_j + h^2 \nabla\phi_{N+1}.\nabla\phi_j) d\underline{x}) U_A, & j = 1 \\ -(\int_{e_{M+2}} (q^2 \phi_{N+2}\phi_j + h^2 \nabla\phi_{N+2}.\nabla\phi_j) d\underline{x}) U_B, & j = m \\ -(\int_{e_{M+3}} (q^2 \phi_{N+3}\phi_j + h^2 \nabla\phi_{N+3}.\nabla\phi_j) d\underline{x}) U_C, & j = N \\ 0 & \text{otherwise} \end{cases} \tag{54}$$

Using the isoparametric representation given by equation (41)

$$b_j^{(n)} = \begin{cases} h\eta_j^{(n)} U_A, & j = 1 \\ h\eta_j^{(n)} U_B, & j = m \\ h\eta_j^{(n)} U_C, & j = N \\ 0 & \text{otherwise} \end{cases} \tag{55}$$

where

$$\eta_j^{(n)} = \begin{cases} \frac{4}{3} - \frac{2}{15} q^2, & j = 1 \\ 1 + \frac{1}{3(2^{n+1}-1)} + \frac{(11-15\times 2^n)}{30(2^{n+1}-1)} q^2, & j = m \text{ or } N. \end{cases} \tag{56}$$

For generation level $n = 1$,

$$b_j^{(1)} = \begin{cases} h(\frac{4}{3} - \frac{2}{15} q^2) U_A, & j = 1 \\ h(\frac{10}{9} - \frac{19}{90} q^2) U_B, & j = 2 \\ h(\frac{10}{9} - \frac{19}{90} q^2) U_C\ , & j = 3 \\ 0 & \text{otherwise} \end{cases}, \tag{57}$$

and for generation level $n = 2$,

$$b_j^{(2)} = \begin{cases} h(\frac{4}{3} - \frac{2}{15}q^2)U_A\ , & j = 1 \\ h(\frac{22}{21} - \frac{7}{30}q^2)U_B\ , & j = 5 \\ h(\frac{22}{21} - \frac{7}{30}q^2)U_C\ , & j = 9 \\ 0 & \text{otherwise} \end{cases} . \tag{58}$$

3.1 Application of the Mechanical boundary conditions

Mechanical and electrical loads will be introduced to the tranducer at its boundaries as displayed in Figure 7. In the mechanical load at the front face of the transducer the governing equation is

$$\rho_L \frac{\partial^2 u_L}{\partial t^2} = Y_L \frac{\partial^2 u_L}{\partial x_L^2}, \tag{59}$$

where u_L is the displacement of the load material, ρ_L is the density and Y_L is the Young's modulus. That is

$$\rho_T \frac{h^2}{Y_T} \frac{\partial^2 u_L}{\partial t^2} = \Big(\frac{\rho_T h^2}{\rho_L Y_T}\Big) Y_L \frac{\partial^2 u_L}{\partial x_L^2} \tag{60}$$

and so, nondimensionalising, gives

$$\frac{\partial^2 u_L}{\partial \theta^2} = \Big(\frac{c_L h}{c_T}\Big)^2 \frac{\partial^2 u_L}{\partial x_L^2} \tag{61}$$

where c_L is the wave speed in the load ($c_L^2 = Y_L/\rho_L$). Taking Laplace transforms gives

$$\frac{\partial^2 \bar{u}_L}{\partial x_L^2} - \Big(\frac{q c_T}{h c_L}\Big)^2 \bar{u}_L = 0. \tag{62}$$

Hence, the displacement in the load is

$$\bar{u}_L = A_L e^{(-q c_T x_L / h c_L)} + B_L e^{(q c_T x_L / h c_L)}, \tag{63}$$

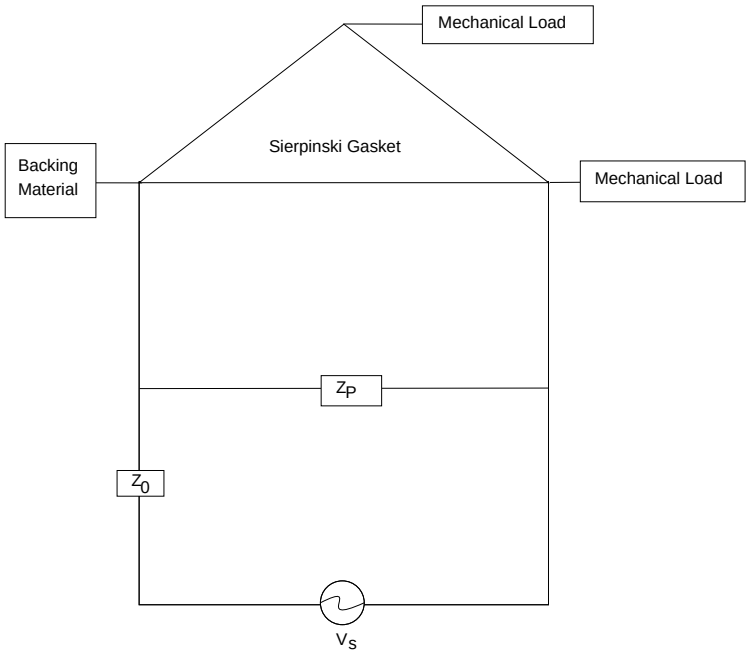

Figure 7: Physical layout of the fractal transducer.

where A_L and B_L are constants. Similarly the displacement in the backing layer (subscript B) is given by

$$\bar{u}_B = A_B e^{(-qc_T x_B/hc_B)} + B_B e^{(qc_T x_B/hc_B)}, \tag{64}$$

where A_B and B_B are constants and c_B is the wave speed in the backing material. As the backing layer is highly attenuative it is assumed that there is only a wave travelling away from the piezoelectric layer ($SG(3)$) interface ($x_B = 0$) in the direction of increasing x_B, and so we set $B_B = 0$. Continuity of displacement at the transducer-mechanical load interface and the symmetry of the $SG(3)$ lattice give

$$U_A = \bar{u}_B(0) = A_B, \tag{65}$$

$$U_B = \bar{u}_L(0) = A_L + B_L, \tag{66}$$

$$U_C = \bar{u}_L(0) = A_L + B_L, \tag{67}$$

where U_A, U_B and U_C are the mechanical displacements at the fictitious vertices A, B and C, respectively. The force F on each vertex is given by $F = A_r T$, where A_r is the cross-sectional area of each edge of the fractal lattice.

From equation (9) only $u_{3,1}$ and $u_{3,1}$ are nonzero and so the only nonzero components of equation (1) are

$$T_{13} = c_{1313}S_{13} + c_{1331}S_{31} - e_{113}E_1, \tag{68}$$

$$T_{31} = c_{3113}S_{13} + c_{3131}S_{31} - e_{131}E_1, \tag{69}$$

$$T_{23} = c_{2323}S_{23} + c_{2332}S_{32} - e_{223}E_2 \tag{70}$$

and

$$T_{32} = c_{3223}S_{23} + c_{3232}S_{32} - e_{232}E_2. \tag{71}$$

That is

$$T_{13} = T_{31} = c_{44}u_{3,1} - e_{24}E_1 \tag{72}$$

and

$$T_{23} = T_{32} = c_{44}u_{3,2} - e_{24}E_2. \tag{73}$$

Similarly, from equation (2), the only nonzero components are

$$D_1 = e_{24}u_{3,1} + \varepsilon_{11}E_1, \tag{74}$$

and

$$D_2 = e_{24}u_{3,2} + \varepsilon_{11}E_2, \tag{75}$$

Given the geometry of the lattice, the positioning of the boundary nodes, and the load conditions there is a line of symmetry given by $x_1 = x_2$ (see Figure 8). Hence $E_1 = E_2 = E$, $u_{3,1} = u_{3,2}$ and $D_1 = D_2 = D$ and so

$$D = e_{24}u_{3,1} + \varepsilon_{11}E. \tag{76}$$

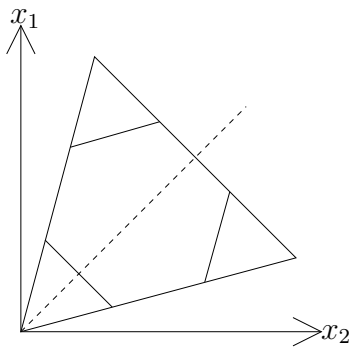

Figure 8: The line of symmetry given by $x_1 = x_2$

That is

$$E = -\zeta S + \frac{D}{\varepsilon} \tag{77}$$

where $\zeta = e_{24}/\varepsilon_{11}$, $S = u_{3,1} = \partial\bar{u}/\partial x$ and $\varepsilon_{11} = \varepsilon$, say. Also, by writing $T_{13} = T$, we have

$$T = c_{44}u_{3,1} - e_{24}E. \tag{78}$$

and substituting equation (76) gives

$$T = \Big(c_{44} + \frac{e_{24}^2}{\varepsilon_{11}}\Big)u_{3,1} - \frac{e_{24}}{\varepsilon_{11}}D. \tag{79}$$

That is

$$T = Y_T S - \zeta D. \tag{80}$$

where $Y_T = c_{44} + e_{24}^2/\varepsilon_{11} = \bar{c}_{44}$ is the piezoelectrically stiffened Young's modulus (the subscripts on the remaining terms being dropped). Hence

$$F = A_r T = A_r Y_T S - \zeta D A_r. \tag{81}$$

By applying an electrical charge Q at one of the transducer-electrical load interfaces then Gauss' law gives $D = Q/A_r$. Since $S = \partial\bar{u}/\partial x$, then

$$F = A_r Y_T \frac{\partial\bar{u}}{\partial x} - \zeta Q. \tag{82}$$

So from the continuity of force we get $F_T(\bar{u}_m) = F_L(\bar{u}_{\partial\Omega}) = F_L(x_L = 0)$. That is

$$A_r Y_T \frac{(U_B - U_m)}{h} - \zeta Q = A_r Y_L \Big(\frac{q c_T}{h c_L}\Big)(-A_L + B_L), \tag{83}$$

and so

$$U_B - U_m - \frac{\zeta Q}{Y_T}\Big(\frac{h}{A_r}\Big) = \frac{Z_L}{Z_T} q(-A_L + B_L), \tag{84}$$

where the mechanical impedance of the load is $Z_L = \rho_L c_L A_r = A_r Y_L / c_L$ and of the transducer is $Z_T = \rho_T c_T A_r$. At each generation level of the Sierpinski gasket transducer the ratio of the cross-sectional area of each edge to its length is denoted by $\xi = A_r/h$. The overall extent of the lattice (L) is fixed and so the length of the edges will steadily decrease and, by fixing ξ, the cross-sectional area will also decrease as the fractal generation level increases (in fact $A_r = \xi L/(2^n - 1)$). Hence, continuity of force gives

$$U_1 - U_A - \frac{\zeta Q}{Y_T \xi} = \frac{Z_B}{Z_T} q(-A_B), \tag{85}$$

$$U_B - U_m - \frac{\zeta Q}{Y_T \xi} = \frac{Z_L}{Z_T} q(-A_L + B_L). \tag{86}$$

From equations (65) and (85) we have that $U_A = \gamma_1 U_1 + \delta_1$ and from equations (66),(67) and (86) we have

$$U_B = \gamma_m U_m + \delta_m = U_C = \gamma_N U_N + \delta_N, \tag{87}$$

where

$$\gamma_j = \begin{cases} (1 - q\frac{Z_B}{Z_T})^{-1}, & j = 1 \\ (1 - q\frac{Z_L}{Z_T})^{-1}, & j = m \text{ or } N \end{cases} \tag{88}$$

and

$$\delta_j = \begin{cases} -\frac{\zeta Q}{Y_T \xi}\Big(1 - q\frac{Z_B}{Z_T}\Big)^{-1}, & j = 1 \\ \Big(1 - q\frac{Z_L}{Z_T}\Big)^{-1}\Big(\frac{\zeta Q}{Y_T \xi} - 2A_L q\frac{Z_L}{Z_T}\Big), & j = m \text{ or } N. \end{cases} \tag{89}$$

Hence, equation (55) becomes

$$b_j^{(n)} = h\bar{\gamma}_j^{(n)} U_j + h\bar{\delta}_j^{\,(n)} \quad j = 1, m \text{ or } N \tag{90}$$

where $\bar{\gamma}_j^{(n)} = \eta_j^{(n)}\gamma_j$ and $\bar{\delta}_j^{\,(n)} = \eta_j^{(n)}\delta_j$. Putting equation (90) into equation (31) gives

$$\hat{A}_{ji}^{(n)} U_i = \bar{\gamma}_j^{(n)} U_j + \bar{\delta}_j^{\,(n)} \tag{91}$$

where $\hat{A} = A/h$. Hence,

$$(\hat{A}_{ji}^{(n)} - \hat{B}_{ji}^{(n)}) U_i = \bar{\delta}_j^{\,(n)}, \quad i = 1, m \text{ or } N \tag{92}$$

where

$$\hat{B}_{ji}^{(n)} = \begin{bmatrix} \bar{\gamma}_1 & 0 & \cdots & & & & \cdots & 0 \\ 0 & 0 & \ddots & & & & & \vdots \\ \vdots & \ddots & \ddots & & & & & \\ & & & 0 & & 0 & & \\ & & & & \bar{\gamma}_m & & & \\ & & & 0 & & 0 & & \\ & & & & & & \ddots & \ddots & \vdots \\ \vdots & & & & & & \ddots & 0 & 0 \\ 0 & \cdots & & & & & \cdots & 0 & \bar{\gamma}_N \end{bmatrix}. \tag{93}$$

That is

$$F_{ji}^{(n)} U_i = \bar{\delta}_j^{\,(n)}, \tag{94}$$

and so

$$U_i = G_{ji}^{(n)} \bar{\delta}_j^{\,(n)}, \tag{95}$$

where

$$G_{ji}^{(n)} = \left(F_{ji}^{(n)}\right)^{-1} = \left(\hat{A}_{ji}^{(n)} - \hat{B}_{ji}^{(n)}\right)^{-1} \tag{96}$$

repesents the Green's transfer matrix.

4 Renormalisation

From equation (95) the desired weightings at each vertex in Ω is given by

$$U_j^{(n)} = G_{j1}^{(n)}\bar{\delta}_1^{(n)} + G_{jm}^{(n)}\bar{\delta}_m^{(n)} + G_{jN}^{(n)}\bar{\delta}_N^{(n)}. \tag{97}$$

In particular we will be interested in $U_1^{(n)}, U_m^{(n)}$ and $U_N^{(n)}$ and so we only need to be able to calculate the pivotal Green's functions $G_{ij}^{(n)}, \quad i,j \in \{1,m,N\}$. If

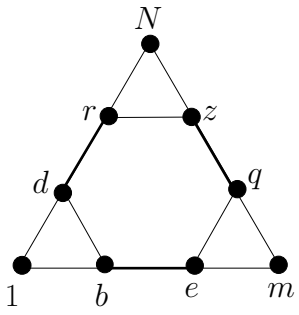

Figure 9: Three Sierpinski Gasket lattices of generation level $n-1$ are connected by the edges in bold $\big((d,r),(b,e)$ and $(q,z)\big)$ to create the Sierpinski Gasket lattice at generation level n.

we temporarily ignore matrix $\hat{B}$ in equation (96) (this matrix originates from consideration of the boundary conditions) then, due to the symmetries of the $SG(3)$ lattice (and hence in matrix $A^{(n)}$), we have

$$\hat{G}_{ii}^{(n)} = \hat{G}_{jj}^{(n)} = \hat{x}, \;\; \text{say}, \quad \text{where} \quad i,j \in \{1,m,N\} \tag{98}$$

(i.e corner-to-same-corner), and

$$\hat{G}_{jk}^{(n)} = \hat{G}_{hk}^{(n)} = \hat{y}, \;\; \text{say}, \quad \text{where} \quad j,k,h \in \{1,m,N\},\, j \neq k \neq h \tag{99}$$

(i.e corner-to-other-corner), where

$$\hat{G}^{(n)} = (\hat{A}^{(n)})^{-1}. \tag{100}$$

For clarity, at level $n+1$, we denote, $X = \hat{G}_{ii}^{(n+1)}$ and $Y = \hat{G}_{ij}^{(n+1)}$ where $i, j, \in \{1, m, N\}$, $i \neq j$. The matrix is symmetrical and consequently, $\hat{G}_{ij}^{(n)} = \hat{G}_{ji}^{(n)}$. From equation (24), since

$$\theta^{(n)} = \frac{c_T}{h^{(n)}} t, \tag{101}$$

then $\mathcal{L} : \theta^{(n)} \rightarrow q^{(n)}$ where $q^{(n)} = i\hat{w}^{(n)} = i2\pi\hat{f}^{(n)} = i2\pi(c_T/h^{(n)})^{-1} f^{(n)}$, $\hat{f}^{(n)}$ is the nondimensionalised natural frequency, $\hat{w}^{(n)}$ is the nondimensionalised angular frequency and $f^{(n)}$ (and $w^{(n)}$) are the dimensionalised equivalents. In order to use the renormalisation approach detailed below then we set $q = q^{(n)} = q^{(n+1)}$. This simply means that the output from the renormalisation methodology (and hence the electrical impedance and transmission/reception sensitivities) at a given q (fixed) is then that quantity at frequency $f^{(n)}$ at generation level n. So when comparing outputs at different generation levels one must ensure that the frequency is scaled appropriately (by $(c_T/h^{(n)})^{-1}$) when re-dimensionalising. An iterative procedure can be developed from equation (34) which can be written

$$\hat{A}_{ji}^{(n)} = \tfrac{8}{5} q^2 I_n - T^{(n)} \tag{102}$$

where

$$T^{(n)} = \beta R^{(n)} - 4I_n, \tag{103}$$

$$R^{(n)} = \bar{R}^{(n-1)} + V^{(n-1)}, \tag{104}$$

$\bar{R}^{(n-1)}$ is a block-diagonal matrix whose three blocks are equal to $R^{(n-1)}$ with

$$R^{(1)} = \begin{bmatrix} 0 & -1 & -1 \\ -1 & 0 & -1 \\ -1 & -1 & 0 \end{bmatrix}, \tag{105}$$

and

$$V^{(n)} = \begin{cases} -1 & \text{if } (h,k) \in \{(b,e),(d,r),(q,z),(e,b),(r,d),(z,q)\} \\ 0 & \text{otherwise} \end{cases}. \tag{106}$$

So, using equations (102) and (103), we can write equation (100) as

$$\begin{aligned} \hat{G}^{(n)} &= \left(\tfrac{8}{5}q^2 I_n - T^{(n)}\right)^{-1} \\ &= \left((\tfrac{8}{5}q^2+4)I_n - \beta R^{(n)}\right)^{-1}. \end{aligned} \tag{107}$$

Hence,

$$(\hat{G}^{(n+1)})^{-1} = (\tfrac{8}{5}q^2+4)I_{n+1} - \beta R^{(n+1)}. \tag{108}$$

Since $\bar{G}^{(n)}$ is a block-diagonal matrix then

$$\begin{aligned} (\bar{G}^{(n)})^{-1} &= \overline{\hat{A}^{(n)}} \\ &= \overline{\left(\tfrac{8}{5}q^2 I_n - T^{(n)}\right)} \\ &= \tfrac{8}{5}q^2 I_{n+1} - \bar{T}^{(n)} \\ &= \tfrac{8}{5}q^2 I_{n+1} - (\beta\bar{R}^{(n)} - 4\bar{I}_n) \\ &= (\tfrac{8}{5}q^2+4)I_{n+1} - \beta\bar{R}^{(n)}. \end{aligned} \tag{109}$$

Now

$$\begin{aligned} I_{n+1} &= \bar{G}^{(n)}(\bar{G}^{(n)})^{-1} \\ &= \bar{G}^{(n)}\left((\tfrac{8}{5}q^2+4)I_{n+1} - \beta\bar{R}^{(n)}\right) \\ &= \bar{G}^{(n)}\left((\tfrac{8}{5}q^2+4)I_{n+1} - \beta(\bar{R}^{(n)} + V^{(n)}) + \beta V^{(n)}\right). \end{aligned}$$

From equations (104) and (108) then

$$\begin{aligned} I_{n+1} &= \bar{G}^{(n)}\left((\hat{G}^{(n+1)})^{-1} + \beta V^{(n)}\right) \\ &= \bar{G}^{(n)}\left((\hat{G}^{(n+1)})^{-1} + \beta V^{(n)}\hat{G}^{(n+1)}(\hat{G}^{(n+1)})^{-1}\right) \\ &= (\bar{G}^{(n)} + \bar{G}^{(n)}\beta V^{(n)}\hat{G}^{(n+1)})(\hat{G}^{(n+1)})^{-1}. \end{aligned} \tag{110}$$

Hence

$$\hat{G}^{(n+1)} = \bar{G}^{(n)} + \beta \bar{G}^{(n)} V^{(n)} \hat{G}^{(n+1)}. \tag{111}$$

To calculate $G_{ij}^{(n)}$ the boundary conditions must be reintroduced. From equations (96),(102) and (103)

$$\begin{aligned}
(G^{(n)})^{-1} &= \hat{A}^{(n)} - \hat{B}^{(n)} \\
&= (\tfrac{8}{5}q^2 I_n - T^{(n)}) - \hat{B}^{(n)} \\
&= \tfrac{8}{5}q^2 I_n - (\beta R^{(n)} - 4I_n) - \hat{B}^{(n)} \\
&= (\tfrac{8}{5}q^2 + 4)I_n - \beta R^{(n)} - \hat{B}^{(n)}.
\end{aligned} \tag{112}$$

Now, from equation (107)

$$\begin{aligned}
I_n &= \hat{G}^{(n)} (\hat{G}^{(n)})^{-1} \\
&= \hat{G}^{(n)} \big((\tfrac{8}{5}q^2 + 4)I_n - \beta R^{(n)} - \hat{B}^{(n)} + \hat{B}^{(n)} \big).
\end{aligned}$$

From equation (112) then,

$$\begin{aligned}
I_n &= \hat{G}^{(n)} \big((G^{(n)})^{-1} + \hat{B}^{(n)} \big) \\
&= \hat{G}^{(n)} \big((G^{(n)})^{-1} + \hat{B}^{(n)} G^{(n)} (G^{(n)})^{-1} \big) \\
&= (\hat{G}^{(n)} + \hat{G}^{(n)} \hat{B}^{(n)} G^{(n)}) (G^{(n)})^{-1}.
\end{aligned} \tag{113}$$

Hence

$$G^{(n)} = \hat{G}^{(n)} + \hat{G}^{(n)} \hat{B}^{(n)} G^{(n)}. \tag{114}$$

4.1 Derivation of the pivotal recursion relationships

The $(i,j)^{th}$ element of the matrix equation (111) can be written as,

$$\hat{G}_{ij}^{(n+1)} = \bar{G}_{ij}^{(n)} + \sum_{h,k} \beta \bar{G}_{ih}^{(n)} V_{hk}^{(n)} \hat{G}_{kj}^{(n+1)}. \tag{115}$$

The system of linear equation in $\hat{G}_{ij}^{(n+1)}$ will create the renormalisation recursion relationships for the pivotal Green's functions. However, these recursions do not include the boundary conditions. Since the subgraphs of Figure 1 only connect to each other at the corners, it will transpire that the recursions in equation (115) only involve two pivotal Green's functions, namely, corner-to-corner and corner-to-same-corner; the so called input/output nodes. To proceed, we now need to determine $\hat{x}$ and $\hat{y}$ as defined in equations (98) and (99). Using equations (106) and (115) we get

$$\begin{aligned}
\hat{G}_{11}^{(n+1)} &= \bar{G}_{11}^{(n)} + \sum_{h,k} \beta \bar{G}_{1h}^{(n)} V_{hk}^{(n)} \hat{G}_{k1}^{(n+1)} \\
&= \hat{G}_{11}^{(n)} + \beta \bar{G}_{1d}^{(n)} V_{dr}^{(n)} \hat{G}_{r1}^{(n+1)} + \beta \bar{G}_{1b}^{(n)} V_{be}^{(n)} \hat{G}_{e1}^{(n+1)} \\
&= \hat{G}_{11}^{(n)} - \beta \hat{G}_{1N}^{(n)} \hat{G}_{r1}^{(n+1)} - \beta \hat{G}_{1m}^{(n)} \hat{G}_{e1}^{(n+1)}.
\end{aligned}$$

That is

$$\hat{X} = \hat{x} - 2\beta \hat{y} \hat{G}_{e1}^{(n+1)}, \tag{116}$$

since we know from equation (106) that $V_{dr}^{(n)} = V_{be}^{(n)} = -1$ and by symmetry $\bar{G}_{1d}^{(n)} = \hat{G}_{1N}^{(n)}$, $\hat{G}_{1N}^{(n)} = \hat{G}_{1m}^{(n)}$ and $\hat{G}_{r1}^{(n+1)} = \hat{G}_{e1}^{(n+1)}$. Similarly,

$$\begin{aligned}
\hat{G}_{e1}^{(n+1)} &= \bar{G}_{e1}^{(n)} + \sum_{h,k} \beta \bar{G}_{eh}^{(n)} V_{hk}^{(n)} \hat{G}_{k1}^{(n+1)} \\
&= \beta \bar{G}_{ee}^{(n)} V_{eb}^{(n)} \hat{G}_{b1}^{(n+1)} + \beta \bar{G}_{eq}^{(n)} V_{qz}^{(n)} \hat{G}_{z1}^{(n+1)} \\
&= -\beta \hat{G}_{11}^{(n)} \hat{G}_{b1}^{(n+1)} - \beta \hat{G}_{1N}^{(n)} \hat{G}_{z1}^{(n+1)}.
\end{aligned}$$

Therefore

$$\hat{G}_{e1}^{(n+1)} = -\beta \hat{x} \hat{G}_{b1}^{(n+1)} - \beta \hat{y} \hat{G}_{z1}^{(n+1)}. \tag{117}$$

Also

$$\begin{aligned}\hat{G}_{b1}^{(n+1)} &= \bar{G}_{b1}^{(n)} + \sum_{h,k} \beta \bar{G}_{bh}^{(n)} V_{hk}^{(n)} \hat{G}_{k1}^{(n+1)} \\ &= \hat{G}_{m1}^{(n)} + \beta \bar{G}_{bb}^{(n)} V_{be}^{(n)} \hat{G}_{e1}^{(n+1)} + \beta \bar{G}_{bd}^{(n)} V_{dr}^{(n)} \hat{G}_{r1}^{(n+1)} \\ &= \hat{y} - \beta \hat{G}_{mm}^{(n)} \hat{G}_{e1}^{(n+1)} - \beta \hat{G}_{mN}^{(n)} \hat{G}_{e1}^{(n+1)}.\end{aligned}$$

Hence

$$\hat{G}_{b1}^{(n+1)} = \hat{y} - \beta \hat{G}_{e1}^{(n+1)} (\hat{x} + \hat{y}), \tag{118}$$

since $\hat{G}_{r1}^{(n+1)} = \hat{G}_{e1}^{(n+1)}$. Finally,

$$\begin{aligned}\hat{G}_{z1}^{(n+1)} &= \bar{G}_{z1}^{(n)} + \sum_{h,k} \beta \bar{G}_{zh}^{(n)} V_{hk}^{(n)} \hat{G}_{k1}^{(n+1)} \\ &= \beta \bar{G}_{zr}^{(n)} V_{rd}^{(n)} \hat{G}_{d1}^{(n+1)} + \beta \bar{G}_{zz}^{(n)} V_{zq}^{(n)} \hat{G}_{q1}^{(n+1)} \\ &= -\beta \hat{G}_{m1}^{(n)} \hat{G}_{b1}^{(n+1)} - \beta \hat{G}_{mm}^{(n)} \hat{G}_{z1}^{(n+1)}.\end{aligned}$$

Therefore

$$\hat{G}_{z1}^{(n+1)} = -\beta \hat{y} \hat{G}_{b1}^{(n+1)} - \beta \hat{x} \hat{G}_{z1}^{(n+1)}, \tag{119}$$

since $\hat{G}_{d1}^{(n+1)} = \hat{G}_{b1}^{(n+1)}$ and $\hat{G}_{q1}^{(n+1)} = \hat{G}_{z1}^{(n+1)}$. Equations (116) to (119) provide four equations in the four unknows $\hat{X}, \hat{G}_{e1}^{(n+1)}, \hat{G}_{b1}^{(n+1)}$ and $\hat{G}_{z1}^{(n+1)}$. Rearranging equation (116) gives (for $\hat{y} \neq 0, \beta \neq 0$)

$$\hat{G}_{e1}^{(n+1)} = \frac{\hat{x} - \hat{X}}{2\beta \hat{y}}, \tag{120}$$

and substituting this into equation (118) gives

$$\hat{G}_{b1}^{(n+1)} = \hat{y} + (\hat{x} + \hat{y}) \Big(\frac{\hat{X} - \hat{x}}{2\hat{y}} \Big). \tag{121}$$

Now rearranging equation (117) gives (for $\hat{y} \neq 0, \beta \neq 0$)

$$\hat{G}_{z1}^{(n+1)} = \frac{-1}{\beta \hat{y}} \Big(\hat{G}_{e1}^{(n+1)} + \beta \hat{x} \hat{G}_{b1}^{(n+1)} \Big), \tag{122}$$

and substituting equations (120) and (121) into equation (122) gives

$$\begin{aligned}\hat{G}_{z1}^{(n+1)} &= \frac{-1}{\beta\hat{y}}\Big[\frac{\hat{x}-\hat{X}}{2\beta\hat{y}} + \beta\hat{x}\hat{y} + \beta\hat{x}(\hat{x}+\hat{y})\Big(\frac{\hat{X}-\hat{x}}{2\hat{y}}\Big)\Big] \\ &= \frac{\hat{X}-\hat{x}}{2\beta^2\hat{y}^2}\big(1-\hat{x}\beta^2(\hat{x}+\hat{y})\big) - \hat{x}, \end{aligned} \tag{123}$$

and substituting equations (121) and (123) into equation (119) gives (where $\hat{X} = \hat{G}_{11}^{(n+1)}$)

$$\Big[\frac{(\hat{X}-\hat{x})}{2\beta^2\hat{y}^2}\big(1-\beta^2\hat{x}(\hat{x}+\hat{y})\big) - \hat{x}\Big](1+\beta\hat{x}) = -\beta\hat{y}\Big[\hat{y} + (\hat{x}+\hat{y})\frac{(\hat{X}-\hat{x})}{2\hat{y}}\Big] \tag{124}$$

so

$$(\hat{X}-\hat{x})\Big[\frac{\big(1-\beta^2\hat{x}(\hat{x}+\hat{y})\big)(1+\beta\hat{x})}{2\beta^2\hat{y}^2} + \frac{\beta\hat{y}(\hat{x}+\hat{y})}{2\hat{y}}\Big] = \hat{x}(1+\beta\hat{x}) - \beta\hat{y}^2 \tag{125}$$

and so

$$(\hat{X}-\hat{x})\Big[(1-\beta^2\hat{x}^2-\beta^2\hat{x}\hat{y})(1+\beta\hat{x}) + \beta^3\hat{y}^2(\hat{x}+\hat{y})\Big] = 2\beta^2\hat{y}^2(\hat{x}+\beta\hat{x}^2-\beta\hat{y}^2) \tag{126}$$

Expanding and factorising we get,

$$\hat{X} = \hat{x} + \frac{2\beta^2\hat{y}^2(\hat{x}+\beta\hat{x}^2-\beta\hat{y}^2)}{(1+\beta\hat{x}+\beta\hat{y})(1-\beta^2\hat{x}^2-\beta\hat{y}+\beta^2\hat{y}^2)}. \tag{127}$$

By substituting this into equations (120),(121) and (123) gives

$$\hat{G}_{e1}^{(n+1)} = \frac{-\beta\hat{y}(\hat{x}+\beta\hat{x}^2-\beta\hat{y}^2)}{(1+\beta\hat{x}+\beta\hat{y})(1-\beta^2\hat{x}^2-\beta\hat{y}+\beta^2\hat{y}^2)}, \tag{128}$$

and

$$\hat{G}_{b1}^{(n+1)} = \frac{\hat{y}(1+\beta\hat{x})}{(1+\beta\hat{x}+\beta\hat{y})(1-\beta^2\hat{x}^2-\beta\hat{y}+\beta^2\hat{y}^2)}, \tag{129}$$

and so

$$\hat{G}_{z1}^{(n+1)} = \frac{-\beta\hat{y}^2}{(1+\beta\hat{x}+\beta\hat{y})(1-\beta^2\hat{x}^2-\beta\hat{y}+\beta^2\hat{y}^2)}. \tag{130}$$

Now, for $\hat{Y} = \hat{G}^{(n+1)}_{m1}$, equation (115) gives

$$\begin{aligned}
\hat{G}^{(n+1)}_{m1} &= \bar{G}^{(n)}_{m1} + \sum_{h,k} \beta \bar{G}^{(n)}_{mh} V^{(n)}_{hk} \hat{G}^{(n+1)}_{k1} \\
&= \beta \bar{G}^{(n)}_{me} V^{(n)}_{eb} \hat{G}^{(n+1)}_{b1} + \beta \bar{G}^{(n)}_{mq} V^{(n)}_{qz} \hat{G}^{(n+1)}_{z1} \\
&= -\beta \hat{G}^{(n)}_{m1} \hat{G}^{(n+1)}_{b1} - \beta \hat{G}^{(n)}_{mN} \hat{G}^{(n+1)}_{z1}.
\end{aligned}$$

Therefore

$$\hat{Y} = -\beta \hat{y} (\hat{G}^{(n+1)}_{b1} + \hat{G}^{(n+1)}_{z1}). \tag{131}$$

Putting equations (129) and (130) into equation (131) gives

$$\hat{Y} = \frac{-\beta \hat{y}^2 (1 + \beta \hat{x} - \beta \hat{y})}{(1 + \beta \hat{x} + \beta \hat{y})(1 - \beta^2 \hat{x}^2 - \beta \hat{y} + \beta^2 \hat{y}^2)}. \tag{132}$$

The boundary conditions can now be considered by rewriting the $(i,j)^{th}$ element of the matrix equation (114) as,

$$G^{(n)}_{ij} = \hat{G}^{(n)}_{ij} + \sum_{h,k} \hat{G}^{(n)}_{ih} \hat{B}^{(n)}_{hk} G^{(n)}_{kj} \tag{133}$$

and so we have,

$$\begin{aligned}
G^{(n)}_{11} &= \hat{G}^{(n)}_{11} + \sum_{h,k} \hat{G}^{(n)}_{ih} \hat{B}^{(n)}_{hk} G^{(n)}_{k1} \\
&= \hat{G}^{(n)}_{11} + \hat{G}^{(n)}_{11} \hat{B}^{(n)}_{11} G^{(n)}_{11} + \hat{G}^{(n)}_{1m} \hat{B}^{(n)}_{mm} G^{(n)}_{m1} + \hat{G}^{(n)}_{1N} \hat{B}^{(n)}_{NN} G^{(n)}_{N1}.
\end{aligned}$$

Therefore

$$x = \hat{x} + \hat{x} \bar{\gamma}_1 x + 2 \hat{y} \bar{\gamma}_m y \tag{134}$$

since $\hat{B}^{(n)}_{11} = \bar{\gamma}_1, \hat{B}^{(n)}_{mm} = \hat{B}^{(n)}_{NN} = \bar{\gamma}_m$ from equation (93). Similarly,

$$\begin{aligned}
G^{(n)}_{1m} &= \hat{G}^{(n)}_{1m} + \sum_{h,k} \hat{G}^{(n)}_{mh} \hat{B}^{(n)}_{hk} G^{(n)}_{k1} \\
&= \hat{G}^{(n)}_{m1} + \hat{G}^{(n)}_{m1} \hat{B}^{(n)}_{11} G^{(n)}_{11} + \hat{G}^{(n)}_{mm} \hat{B}^{(n)}_{mm} G^{(n)}_{m1} + \hat{G}^{(n)}_{mN} \hat{B}^{(n)}_{NN} G^{(n)}_{N1}.
\end{aligned}$$

Hence

$$y = \hat{y} + \hat{y}\bar{\gamma}_1 x + \hat{x}\bar{\gamma}_m y + \hat{y}\bar{\gamma}_m y. \tag{135}$$

Letting $G^{(n)}_{mm} = z$ and $G^{(n)}_{mN} = w$ then,

$$\begin{aligned} G^{(n)}_{mm} &= \hat{G}^{(n)}_{mm} + \sum_{h,k} \hat{G}^{(n)}_{mh}\hat{B}^{(n)}_{hk}G^{(n)}_{km} \\ &= \hat{G}^{(n)}_{mm} + \hat{G}^{(n)}_{m1}\hat{B}^{(n)}_{11}G^{(n)}_{1m} + \hat{G}^{(n)}_{mm}\hat{B}^{(n)}_{mm}G^{(n)}_{mm} + \hat{G}^{(n)}_{mN}\hat{B}^{(n)}_{NN}G^{(n)}_{Nm}. \end{aligned}$$

Therefore

$$z = \hat{x} + \hat{y}\bar{\gamma}_1 y + \hat{x}\bar{\gamma}_m z + \hat{y}\bar{\gamma}_m w. \tag{136}$$

Finally,

$$\begin{aligned} G^{(n)}_{mN} &= \hat{G}^{(n)}_{mN} + \sum_{h,k} \hat{G}^{(n)}_{mh}\hat{B}^{(n)}_{hk}G^{(n)}_{kN} \\ &= \hat{G}^{(n)}_{mN} + \hat{G}^{(n)}_{m1}\hat{B}^{(n)}_{11}G^{(n)}_{1N} + \hat{G}^{(n)}_{mm}\hat{B}^{(n)}_{mm}G^{(n)}_{mN} + \hat{G}^{(n)}_{mN}\hat{B}^{(n)}_{NN}G^{(n)}_{NN}. \end{aligned}$$

Hence

$$w = \hat{y} + \hat{y}\bar{\gamma}_1 y + \hat{x}\bar{\gamma}_m w + \hat{y}\bar{\gamma}_m z. \tag{137}$$

the four equations (134),(135),(136) and (137) can be solved to express x, y, w, z in terms of $\hat{x}, \hat{y}, \bar{\gamma}_1, \bar{\gamma}_m$. Solving equations (134),(135) for x and y gives

$$x = \frac{\hat{x} + 2\hat{y}\bar{\gamma}_m y}{1 - \hat{x}\bar{\gamma}_1}. \tag{138}$$

Substituting equation (138) into equation (135) gives

$$y = \hat{y} + \hat{y}\bar{\gamma}_1\big(\frac{\hat{x} + 2\hat{y}\bar{\gamma}_m y}{1 - \hat{x}\bar{\gamma}_1}\big) + \hat{x}\bar{\gamma}_m y + \hat{y}\bar{\gamma}_m y. \tag{139}$$

Therefore

$$y = \frac{\hat{y}}{\big(1 - \hat{x}\bar{\gamma}_1\big)\big(1 - \bar{\gamma}_m(\hat{x} + \hat{y})\big) - 2\hat{y}^2\bar{\gamma}_1\bar{\gamma}_m}. \tag{140}$$

Rearranging equation (136) we get

$$z(1 - \hat{x}\bar{\gamma}_m) = \hat{x} + \hat{y}\bar{\gamma}_1 y + \hat{y}\bar{\gamma}_m w. \tag{141}$$

That is

$$z = \frac{\hat{x} + \hat{y}\bar{\gamma}_1 y + \hat{y}\bar{\gamma}_m w}{1 - \hat{x}\bar{\gamma}_m}. \tag{142}$$

Substituting equation (142) into (137) gives

$$w(1 - \hat{x}\bar{\gamma}_m) = \hat{y} + \hat{y}\bar{\gamma}_1 y + \hat{y}\bar{\gamma}_m\big(\frac{\hat{x} + \hat{y}\bar{\gamma}_1 y + \hat{y}\bar{\gamma}_m w}{1 - \hat{x}\bar{\gamma}_m}\big) \tag{143}$$

which can be written as

$$w = \frac{\hat{y}(1 + \bar{\gamma}_1 y)}{1 - \hat{x}\bar{\gamma}_m} + \frac{\hat{y}\bar{\gamma}_m\big(\hat{x} + \hat{y}(\bar{\gamma}_1 y + \bar{\gamma}_m w)\big)}{(1 - \hat{x}\bar{\gamma}_m)^2}. \tag{144}$$

Therefore

$$w = \frac{\hat{y}\big(1 + \bar{\gamma}_1 y(1 + \bar{\gamma}_m(\hat{y} - \hat{x}))\big)}{(\hat{x}\bar{\gamma}_m - 1 + \hat{y}\bar{\gamma}_m)(\hat{x}\bar{\gamma}_m - 1 - \hat{y}\bar{\gamma}_m)} \tag{145}$$

5 Electrical Impedance and Transmission Sensitivity

In transmission mode there is no force incident on the front face of the transducer and so $A_L = 0$. Consider one edge in the lattice connecting vertex 1 to vertex N, and apply a charge Q at vertex N. The voltage V is defined as follows

$$V = \int_0^L E dx \tag{146}$$

and using equation (77)

$$\begin{aligned} V &= \int_0^L \big(-\zeta S + \frac{D}{\varepsilon}\big) dx \\ &= \int_0^L \big(-\zeta \frac{\partial \bar{u}}{\partial x} + \frac{D}{\varepsilon}\big) dx. \end{aligned}$$

Now using Gauss' law

$$\begin{aligned} V &= -\zeta(U_N - U_1) + \frac{QL}{A_r \varepsilon} \\ &= -\zeta(U_N - U_1) + \frac{Q}{C_0} \end{aligned} \tag{147}$$

where the capacitance is given by $C_0 = A_r\varepsilon/L$. Since the charge $Q = \int I dt = \sqrt{(\rho_T/Y_T)}\, h \int I d\theta$ where $\theta = c_T t/h$ then, by taking Laplace transforms gives

$$Q = \sqrt{\frac{\rho_T}{Y_T}} h \frac{I}{q}. \tag{148}$$

That is

$$I = \frac{qQY_T\xi}{Z_T}, \tag{149}$$

where $Z_T = \sqrt{Y_T\rho_T}A_r$. The electrical impedance of the device, denoted by Z_E, is given by

$$\begin{aligned} Z_E = \frac{V}{I} &= \frac{V_E}{qQ}\Big(\frac{Y_T\xi}{Z_T}\Big)^{-1} \\ &= \Big(\frac{-\zeta C_0(U_N - U_1) + Q}{QC_0q}\Big)\Big(\frac{Y_T\xi}{Z_T}\Big)^{-1} \\ &= \Big(\frac{Z_T}{C_0qY_T\xi}\Big)\Big(1 - \frac{\zeta C_0(U_N - U_1)}{Q}\Big). \end{aligned} \tag{150}$$

Now using equation (97)

$$\begin{aligned} U_1^{(n)} &= G_{11}^{(n)}\bar{\delta}_1^{(n)} + G_{1m}^{(n)}\bar{\delta}_m^{(n)} + G_{1N}^{(n)}\bar{\delta}_N^{(n)} \\ &= G_{11}^{(n)}\bar{\delta}_1^{(n)} + \bar{\delta}_m^{(n)}(G_{1m}^{(n)} + G_{1N}^{(n)}) \\ &= G_{11}^{(n)}\bar{\delta}_1^{(n)} + 2G_{1m}^{(n)}\bar{\delta}_m^{(n)} \end{aligned}$$

since $G_{1m}^{(n)} = G_{1N}^{(n)}$ and $\bar{\delta}_N^{(n)} = \bar{\delta}_m^{(n)}$. From equation (90)

$$U_1^{(n)} = -\frac{\zeta Q}{Y_T\xi}\Big(\eta_1^{(n)}\Big(1 - q\frac{Z_B}{Z_T}\Big)^{-1}G_{11}^{(n)} - \eta_m^{(n)}\Big(1 - q\frac{Z_L}{Z_T}\Big)^{-1}2G_{1m}^{(n)}\Big). \tag{151}$$

Similarly,

$$\begin{aligned} U_N^{(n)} &= G_{N1}^{(n)}\bar{\delta}_1^{(n)} + G_{Nm}^{(n)}\bar{\delta}_m^{(n)} + G_{NN}^{(n)}\bar{\delta}_N^{(n)} \\ &= G_{N1}^{(n)}\bar{\delta}_1^{(n)} + \bar{\delta}_m^{(n)}(G_{Nm}^{(n)} + G_{NN}^{(n)}). \end{aligned}$$

Therefore

$$U_N^{(n)} = -\frac{\zeta Q}{Y_T\xi}\Big(\eta_1^{(n)}\Big(1 - q\frac{Z_B}{Z_T}\Big)^{-1}G_{N1}^{(n)} - \eta_m^{(n)}\Big(1 - q\frac{Z_L}{Z_T}\Big)^{-1}(G_{Nm}^{(n)} + G_{NN}^{(n)})\Big). \tag{152}$$

Note that in equation (89) $\delta_m^{(n)} = \zeta Q/(Y_T\xi)\big(1-q(Z_L/Z_T)\big)^{-1}$ since $A_L = 0$. Substituting equations (151) and (152) into equation (150) gives

$$\begin{aligned} Z_E &= \Big(\frac{Z_T}{C_0 q Y_T \xi}\Big)\Big(1+\frac{\zeta^2 C_0}{Y_T\xi}\Big(\Big(1-q\frac{Z_B}{Z_T}\Big)^{-1}\eta_1^{(n)}(G_{N1}^{(n)}-G_{11}^{(n)}) \\ &\quad +\Big(1-q\frac{Z_L}{Z_T}\Big)^{-1}\eta_m^{(n)}(-G_{Nm}^{(n)}-G_{NN}^{(n)}+2G_{1m}^{(n)})\Big)\Big) \\ &= \Big(\frac{Z_T}{C_0 q Y_T \xi}\Big)\Big(1+\frac{\zeta^2 C_0}{Y_T\xi}(\sigma_1+\sigma_2)\Big). \end{aligned} \tag{153}$$

Hence, the non-dimensionalised electrical impedance is given by

$$\hat{Z}_E(f;n) = Z_E/Z_0 = \Big(\frac{Z_T}{C_0 q Y_T \xi Z_0}\Big)\Big(1+\frac{\zeta^2 C_0}{Y_T\xi}(\sigma_1+\sigma_2)\Big) \tag{154}$$

where $\sigma_1 = \big(1-q(Z_B/Z_T)\big)^{-1}\eta_1^{(n)}(G_{N1}^{(n)}-G_{11}^{(n)})$ and $\sigma_2 = \big(1-q(Z_L/Z_T)\big)^{-1}\eta_m^{(n)}(-G_{Nm}^{(n)}-G_{NN}^{(n)}+2G_{1m}^{(n)})$ and Z_0 is series electrical load. This can be compared with the non-dimensionalised from for the electrical impedance of the standard (Euclidean) transducer [18]

$$\bar{Z}_E = \frac{1}{qC_0Z_0}\Big(1-\frac{\zeta^2 C_0}{2qZ_T}(K_F T_F + K_B T_B)\Big), \tag{155}$$

where T_F and T_B are non-dimensional transmission coefficients and K_F and K_B are also non-dimensional and are given by

$$K_F = \frac{(1-e^{-q\tau})(1-R_B e^{-q\tau})}{(1-R_F R_B e^{-2q\tau})} \tag{156}$$

and

$$K_B = \frac{(1-e^{-q\tau})(1-R_F e^{-q\tau})}{(1-R_F R_B e^{-2q\tau})} \tag{157}$$

where R_F and R_B are non-dimensionalised reflection coefficients and τ is the wave transit time across the device. In order to calculate the transmission sensitivity, consider the circuit shown in Figure 7. The current across the transducer I is given by [18]

$$I = \frac{aV}{Z_E+b} \tag{158}$$

where

$$a = \frac{Z_q}{Z_0 + Z_q} \text{ and } b = \frac{Z_0 Z_q}{Z_0 + Z_q}. \tag{159}$$

Note, V denotes the voltage supply. Continuity of force at the front face given by equation (83) and continuity of displacement given by equation (67) (with $A_L = 0$) gives

$$F = F_L(x_L = 0) = A_r Y_L \Big(\frac{qc_T}{hc_L}\Big) U_C. \tag{160}$$

Substituting equation (87) into equation (160) gives

$$F = A_r Y_L \Big(\frac{qc_T}{hc_L}\Big)(\gamma_m U_m + \delta_m). \tag{161}$$

From equations (88) and (89) with $A_L = 0$ then

$$F = A_r Y_L \Big(\frac{qc_T}{hc_L}\Big)\Big(\Big(1 - q\frac{Z_L}{Z_T}\Big)^{-1} U_m + \frac{\zeta Q}{Y_T \xi}\Big(1 - q\frac{Z_L}{Z_T}\Big)^{-1}\Big). \tag{162}$$

Therefore

$$F = \frac{\xi Y_L q c_T}{c_L}\Big(1 - q\frac{Z_L}{Z_T}\Big)^{-1}\Big(U_m + \frac{\zeta Q}{Y_T \xi}\Big), \tag{163}$$

since $\xi = A_r/h$. To obtain U_m we make use of equation (97) to obtain

$$U_m^{(n)} = \frac{\zeta Q}{Y_T \xi}\Big(- \eta_1^{(n)}\Big(1 - q\frac{Z_B}{Z_T}\Big)^{-1} G_{m1}^{(n)} + \eta_m^{(n)}\Big(1 - q\frac{Z_L}{Z_T}\Big)^{-1}(G_{mm}^{(n)} + G_{mN}^{(n)})\Big). \tag{164}$$

Therefore equation (163) becomes

$$\begin{aligned} F &= \frac{Y_L q c_T}{c_L}\Big(\frac{\zeta Q}{Y_T}\Big)\Big(1 - q\frac{Z_L}{Z_T}\Big)^{-1}\Big(- \eta_1^{(n)}\Big(1 - q\frac{Z_B}{Z_T}\Big)^{-1} G_{m1}^{(n)} + \\ &\quad \eta_m^{(n)}\Big(1 - q\frac{Z_L}{Z_T}\Big)^{-1}(G_{mm}^{(n)} + G_{mN}^{(n)}) + 1\Big). \end{aligned} \tag{165}$$

From equations (149) and (158)

$$Q = \frac{I Z_T}{q Y_T \xi} = \frac{aV}{(Z_E + b)}\frac{Z_T}{q Y_T \xi}, \tag{166}$$

then substituting in equation (165) gives

$$\begin{aligned}\frac{F}{V} &= \frac{Z_L\zeta a}{(Z_E+b)Y_T\xi}\Big(1-q\frac{Z_L}{Z_T}\Big)^{-1}\Big(-\eta_1^{(n)}\Big(1-q\frac{Z_B}{Z_T}\Big)^{-1}G_{m1}^{(n)}+\\ &\quad \eta_m^{(n)}\Big(1-q\frac{Z_L}{Z_T}\Big)^{-1}(G_{mm}^{(n)}+G_{mN}^{(n)})+1\Big),\end{aligned} \tag{167}$$

and so

$$\frac{F}{V}=\frac{Z_L\zeta a}{(Z_E+b)Y_T\xi}K^{(n)} \tag{168}$$

where

$$K^{(n)}=\Big(1-q\frac{Z_L}{Z_T}\Big)^{-1}\Big(-\eta_1^{(n)}\Big(1-q\frac{Z_B}{Z_T}\Big)^{-1}G_{m1}^{(n)}+\eta_m^{(n)}\Big(1-q\frac{Z_L}{Z_T}\Big)^{-1}(G_{mm}^{(n)}+G_{mN}^{(n)})+1\Big). \tag{169}$$

The non-dimensionalised transmission sensitivity ψ is then given by

$$\psi(f;n)=\Big(\frac{F}{V}\Big)/\zeta C_0=\frac{aZ_L}{(Z_E+b)Y_T\xi C_0}K^{(n)}. \tag{170}$$

This expression can be compared to the equivalent transmission sensitivity $\bar{\psi}$ in a homogeneous (Euclidean) domain [10]

$$\begin{aligned}\bar{\psi}(f) &= \Big(\frac{\bar{F}}{V}\Big)/\zeta C_0\\ &= -\frac{aA_F\lambda K_F}{2C_0}\Big(1-\frac{\zeta^2\lambda(K_FT_F+K_BT_B)}{2qZ_T}\Big)^{-1},\end{aligned} \tag{171}$$

where $\lambda=C_0/(1+qC_0b)$ and $A_F=2Z_L/(Z_L+Z_T)$ are dimensionless constants.

6 Reception Sensitivity

In reception mode A_L is now non zero because the front face will be subject to a force (given by the incoming signal). From equations (89) and (95)

$$U_1^{(n)}=-\frac{\zeta Q}{Y_T\xi}\eta_1^{(n)}\Big(1-q\frac{Z_B}{Z_T}\Big)^{-1}G_{11}^{(n)}+\Big(\frac{\zeta Q}{Y_T\xi}-2A_Lq\frac{Z_L}{Z_T}\Big)\eta_m^{(n)}\Big(1-q\frac{Z_L}{Z_T}\Big)^{-1}2G_{1m}^{(n)} \tag{172}$$

and

$$U_N^{(n)} = -\frac{\zeta Q}{Y_T\xi}\eta_1^{(n)}\Big(1-q\frac{Z_B}{Z_T}\Big)^{-1}G_{N1}^{(n)}+\Big(\frac{\zeta Q}{Y_T\xi}-2A_Lq\frac{Z_L}{Z_T}\Big)\eta_m^{(n)}\Big(1-q\frac{Z_L}{Z_T}\Big)^{-1}(G_{Nm}^{(n)}+G_{NN}^{(n)}). \tag{173}$$

Putting these into equation (147) gives

$$\begin{aligned} V &= \Big[\frac{\zeta^2 Q}{Y_T\xi}\eta_1^{(n)}\Big(1-q\frac{Z_B}{Z_T}\Big)^{-1}(G_{N1}^{(n)}-G_{11}^{(n)})+\Big(\frac{\zeta^2Q}{Y_T\xi}-2\zeta A_Lq\frac{Z_L}{Z_T}\Big)\eta_m^{(n)}\Big(1-q\frac{Z_L}{Z_T}\Big)^{-1} \\ &\quad (2G_{1m}^{(n)}-G_{Nm}^{(n)}-G_{NN}^{(n)})\Big]+\frac{Q}{C_0}. \end{aligned}$$

Then

$$V = \Big[\frac{\zeta^2Q}{Y_T\xi}\sigma_1+\frac{\zeta^2Q}{Y_T\xi}\sigma_2-2\zeta A_Lq\frac{Z_L}{Z_T}\sigma_2\Big]+\frac{Q}{C_0} \tag{174}$$

and so

$$V = Q\Big(\frac{\zeta^2}{Y_T\xi}(\sigma_1+\sigma_2)+\frac{1}{C_0}\Big)-2\zeta A_Lq\frac{Z_L}{Z_T}\sigma_2. \tag{175}$$

From equation (82) the force in the load ($\zeta = 0$) is given by

$$F = A_rY_L\frac{\partial\bar{u}_L}{\partial x}. \tag{176}$$

From equation (63)

$$\frac{\partial\bar{u}_L}{\partial x} = \Big(\frac{qc_T}{hc_L}\Big)\Big(B_Le^{(-qc_Tx_L/hc_L)}-A_Le^{(-qc_Tx_L/hc_L)}\Big), \tag{177}$$

and so, at $x_L = 0$,

$$\frac{\partial\bar{u}_L}{\partial x} = \Big(\frac{qc_T}{hc_L}\Big)\Big(-A_L\Big), \tag{178}$$

since in receiving mode $B_L = 0$. Substituting this equation into equation (176) we get

$$F = \frac{\xi qc_TZ_L}{A_r}\Big(-A_L\Big) \tag{179}$$

since $\xi = A_r/h$ and $Z_L = Y_LA_r/c_L$. Then

$$A_L = \frac{-FA_r}{\xi qc_TZ_L}. \tag{180}$$

Therefore equation (175) becomes

$$V = \frac{aVZ_T}{(Z_E+b)qY_T\xi}\Big(\frac{\zeta^2}{Y_T\xi}(\sigma_1+\sigma_2)+\frac{1}{C_0}\Big)+\frac{2F\zeta\sigma_2}{\xi Y_T}, \tag{181}$$

using equation (166) and since $Y_T = Z_T c_T/A_r$, and so

$$V\Big[1-\frac{aZ_T}{(Z_E+b)qY_T\xi}\Big(\frac{\zeta^2}{Y_T\xi}(\sigma_1+\sigma_2)+\frac{1}{C_0}\Big)\Big] = \frac{2F\zeta\sigma_2}{\xi Y_T}, \tag{182}$$

and hence

$$\frac{V}{F} = \frac{2\zeta\sigma_2}{\xi Y_T}\Big(1-\frac{\zeta^2 aZ_T(\sigma_1+\sigma_2)}{(Z_E+b)qY_T^2\xi^2}-\frac{aZ_T}{(Z_E+b)qY_T\xi C_0}\Big)^{-1}. \tag{183}$$

The non-dimensionalised reception sensitivity ϕ is then

$$\begin{aligned}\phi(f;n) &= \Big(\frac{V}{F}\Big)(e_{24}L)\\ &= \frac{2\zeta e_{24}L\sigma_2}{\xi Y_T}\Big(1-\frac{\zeta^2 aZ_T(\sigma_1+\sigma_2)}{(Z_E+b)qY_T^2\xi^2}-\frac{aZ_T}{(Z_E+b)qY_T\xi C_0}\Big)^{-1}.\end{aligned} \tag{184}$$

This expression can be compared to the equivalent reception sensitivity $\bar{\phi}$ in the Euclidean case [9]

$$\bar{\phi} = \Big(\frac{\bar{V}}{F}\Big)(e_{24}L) = \Big(\frac{-\zeta T_F K_F H e_{24}L}{qZ_T}\Big)\Big(1-\frac{\zeta^2 H(K_F T_F+K_B T_B)}{2q^2 Z_T Z_E}\Big)^{-1}, \tag{185}$$

where $H = qC_0b/(1+qC_0b)$. Having derived expressions for the main operating characteristics of this new device it is necessary to compare these with those of a standard device to assess any practical benefits arising from this novel design.

7 Steady State Solution

The fractal case arises when we allow the generation level n to tend to infinity and we assume that the recursion relationships converge to a steady state (we denote these steady state solutions by a $*$ superscript). Note we will examine the convergence of these recursion relationships later when we consider the pre-fractal $SG(3)$ transducer (finite generation levels).

Case A: $\hat{y}^* = 0$

If $\hat{y}^* = 0$ then equation (116) is automatically satisfied (since $\hat{X} = \hat{x} = \hat{x}^*$) and from equations (117) and (118) we get

$$\hat{G}^*_{e1} = -\beta \hat{x}^* \hat{G}^*_{b1} \tag{186}$$

and

$$\hat{G}^*_{b1} = -\beta \hat{x}^* \hat{G}^*_{e1}. \tag{187}$$

Substituting equation (186) into equation (187) gives

$$\hat{G}^*_{b1}(1 - \beta^2 \hat{x}^{*2}) = 0. \tag{188}$$

Therefore $\hat{G}^*_{b1} = 0$ or $\hat{x}^* = \pm 1/\beta$. In the former case then $\hat{G}^*_{e1} = 0$ and in the latter case $\hat{G}^*_{b1} = \mp \hat{G}^*_{e1}$. From equation (119) we get

$$\hat{G}^*_{z1}(1 + \beta \hat{x}^*) = 0. \tag{189}$$

Therefore $\hat{G}^*_{z1} = 0$ or $\hat{x}^* = -1/\beta$. Now bringing in the boundary conditions equation (142) gives

$$z = \frac{\hat{x}^*}{1 - \hat{x}^* \bar{\gamma}_m} \tag{190}$$

where $\hat{x}^* \neq 1/\bar{\gamma}_m$. From equation (138) we get

$$x = \frac{\hat{x}^*}{1 - \hat{x}^* \bar{\gamma}_1} \tag{191}$$

where $\hat{x}^* \neq 1/\bar{\gamma}_1$. From equation (135) we get

$$y = \hat{x}^* \bar{\gamma}_m y. \tag{192}$$

That is

$$y = 0 \tag{193}$$

since $\hat{x}^* \neq 1/\bar{\gamma}_m$. From equation (137) we get

$$w = \hat{x}^* \bar{\gamma}_m w. \tag{194}$$

That is

$$w = 0 \tag{195}$$

since $\hat{x}^* \neq 1/\bar{\gamma}_m$. In the case where $\hat{G}^*_{b1} = \hat{G}^*_{e1} = \hat{G}^*_{z1} = 0$ we denote the solution as $x^* = \chi$, $\chi \in \mathbb{C}$ and in the case where $\hat{x}^* = \pm 1/\beta$ we denote the solutions as $\hat{G}^*_{b1} = \mp\lambda$, $\hat{G}^*_{e1} = \mp\lambda$ and $\hat{G}^*_{z1} = \theta$ (or 0 when $\hat{x}^* = 1/\beta$) where $\lambda, \theta \in \mathbb{C}$. The full set of solutions are summarised in the table below.

Case	$\hat{x}^*$	$\hat{y}^*$	$\hat{G}^*_{b1}$	$\hat{G}^*_{e1}$	$\hat{G}^*_{z1}$	x	y	w	z	note
A1	$\frac{-1}{\beta}$	0	λ	$-\lambda$	θ	$\frac{-1}{\beta+\bar{\gamma}_1}$	0	0	$\frac{-1}{\beta+\bar{\gamma}_m}$	$\beta \neq \bar{\gamma}_1, \beta \neq \bar{\gamma}_m$
A2	$\frac{1}{\beta}$	0	$-\lambda$	λ	0	$\frac{1}{\beta-\bar{\gamma}_1}$	0	0	$\frac{1}{\beta-\bar{\gamma}_m}$	$\beta \neq \bar{\gamma}_1, \beta \neq \bar{\gamma}_m$
A3	χ	0	0	0	0	$\frac{\chi}{1-\chi\bar{\gamma}_1}$	0	0	$\frac{\chi}{1-\chi\bar{\gamma}_m}$	$\bar{\gamma}_1 \neq \frac{1}{\chi}, \bar{\gamma}_m \neq \frac{1}{\chi}, \chi \neq \pm\frac{1}{\beta}$

Case B: $\hat{y}^* \neq 0$

If $\hat{y}^* \neq 0$ then from equation (116) we get

$$-2\beta\hat{y}^*\hat{G}^*_{e1} = 0 \tag{196}$$

since $\hat{X} = \hat{x} = \hat{x}^*$ and $\hat{Y} = \hat{y} = \hat{y}^*$. That is

$$\hat{G}^*_{e1} = 0 \tag{197}$$

since $\beta \neq 0, \hat{y}^* \neq 0$. Substituting this into equations (117) and (118) we get

$$\hat{x}^*\hat{G}^*_{b1} + \hat{y}^*\hat{G}^*_{z1} = 0 \tag{198}$$

and

$$\hat{G}^*_{b1} = \hat{y}^*. \tag{199}$$

Substituting equation (199) into equation (198) gives

$$\hat{G}^*_{z1} = -\hat{x}^*. \tag{200}$$

Substituting equations (199) and (200) into equation (119) gives

$$\hat{x}^* + \beta\hat{x}^{*2} - \beta\hat{y}^{*2} = 0. \tag{201}$$

Note that $\hat{x}^* \neq 0$ since this would imply that $\hat{y}^*$ was zero. Also substituting equations (199) and (200) into equation (131) gives

$$\hat{y}^* = -\beta\hat{y}^*(\hat{y}^* - \hat{x}^*). \tag{202}$$

That is

$$\hat{y}^* = \hat{x}^* - \frac{1}{\beta}. \tag{203}$$

Putting this into equation (201) gives

$$\hat{x}^* = \frac{1}{3\beta}. \tag{204}$$

Putting this into equation (203) gives

$$\hat{y}^* = \frac{-2}{3\beta}. \tag{205}$$

Now putting equations (204) and (205) into the boundary conditions equation (140) gives

$$y = \frac{-2\beta}{3\beta^2 - 3\bar{\gamma}_1\bar{\gamma}_m + \beta(-\bar{\gamma}_1 + \bar{\gamma}_m)}. \tag{206}$$

Putting equations (204),(205) and (206) into equations (138) and (145) gives

$$x = \frac{\beta + 3\bar{\gamma}_m}{3\beta^2 - \beta\bar{\gamma}_1 + \beta\bar{\gamma}_m - 3\bar{\gamma}_1\bar{\gamma}_m} \tag{207}$$

and

$$w = \frac{-2\beta(\beta - \bar{\gamma}_1)}{(\beta - \bar{\gamma}_m)\big(3\beta^2 - 3\bar{\gamma}_1\bar{\gamma}_m + \beta(-\bar{\gamma}_1 - \bar{\gamma}_m)\big)}. \tag{208}$$

Substituting equations (204),(205),(206) and (208) into equation (142) gives

$$z = \frac{\beta^2 - 3\bar{\gamma}_1\bar{\gamma}_m + \beta(\bar{\gamma}_1 + \bar{\gamma}_m)}{(\beta - \bar{\gamma}_m)\big(3\beta^2 - 3\bar{\gamma}_1\bar{\gamma}_m + \beta(-\bar{\gamma}_1 + \bar{\gamma}_m)\big)}. \tag{209}$$

Note that from equation (101), $h^{(n)} \to 0$ and $q^{(n)} \to 0$ as $n \to \infty$, and so from equation (154) the non-dimensionalised electrical impedance tends to infinity ($(\hat{Z}_E(f;n)) \to \infty$), from equation (170) the non-dimensionalised transmission sensitivity tends to zero ($\psi(f;n) \to 0$), and from equation (88) $\gamma_j \to 1$ and from equation (90) $\bar{\gamma}_j \to \eta_j^*$. From equation (56) we get

$$\eta_j^* = \begin{cases} \frac{4}{3}, & j = 1 \\ 1, & j = m \text{ or } N. \end{cases} \tag{210}$$

From equation (184) the non-dimensionalised reception sensitivity is

$$\phi^*(f;n) = \frac{2\zeta e_{24} L \sigma_2^*}{\xi Y_T (1-a)}, \tag{211}$$

where

$$\sigma_2^* = \begin{cases} \frac{1}{1+\beta}, & \text{in case A1} \\ \frac{1}{1-\beta}, & \text{in case A2} \\ \frac{\chi}{\chi - 1}, & \text{in case A3} \\ \frac{-3(3\beta+4)}{9\beta^2+\beta-12}, & \text{in case B} \end{cases} \tag{212}$$

8 Results

From a practical perspective, these fractal transducers will only be able to be manufactured at low generation levels. The formulation presented above will

allow us to compare the fractal design with a conventional (Euclidean) design in terms of the key operating characteristics of the reception and transmission sensitivity spectra. Within each, the presence of higher amplitudes, multiple resonances, and improved bandwidth (the range of frequencies over which the performance exceeds a certain decibel level) are the key performance indicators of interest in this section.

8.1 Electrical Impedance and Transmission/Reception Sensitivities

Let us start by examining the performance of the first generation lattice ($n = 1$).

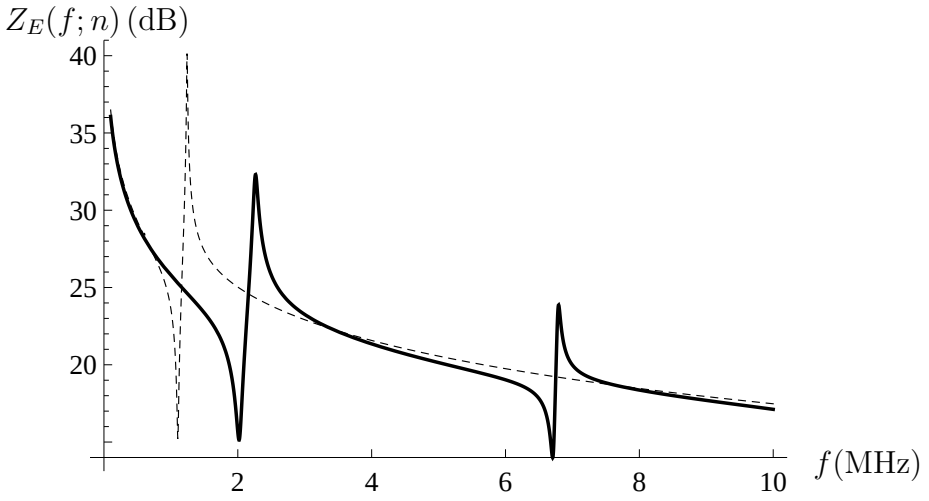

Figure 10: Non-dimensionalised electrical impedance (equation (154)) versus frequency for the $SG(3)$ lattice transducer at fractal generation level $n = 1$ (dashed line). The non-dimensionalised electrical impedance of the standard (Euclidean) transducer (equation (155)) is plotted for comparison (full line). Parameter values are given in Table 5.

Figure 10 shows that the electrical impedance of the fractal lattice has its first resonance at around 1 MHz (at a lower frequency than the Euclidean case) and that the higher frequency resonances are absent.

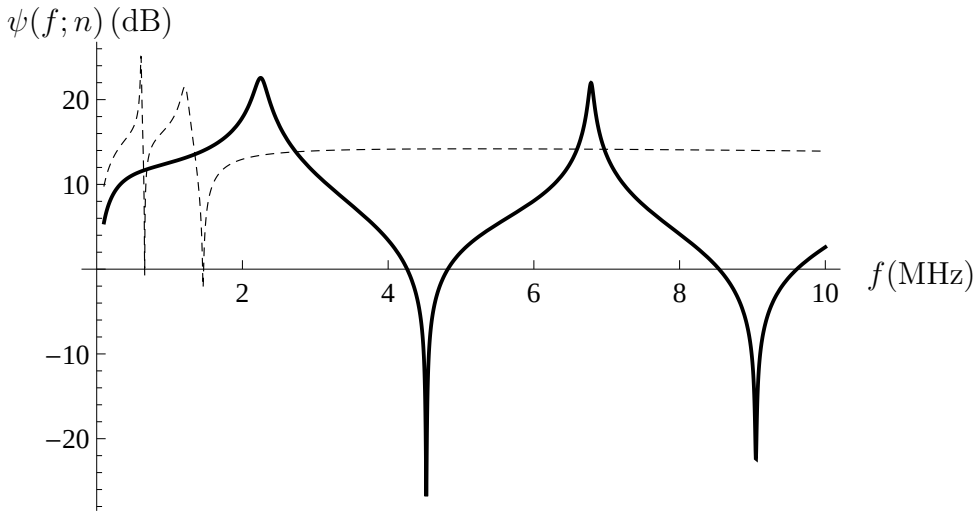

Figure 11: Non-dimensionalised transmission sensitivity (equation (170)) versus frequency for the $SG(3)$ lattice transducer at fractal generation level $n = 1$ (dashed line). The non-dimensionalised transmission sensitivity of the standard (Euclidean) transducer (equation (171)) is plotted for comparison (full line). Parameter values are given in Table 5.

The transmission sensitivity has a maximum amplitude (gain) that is higher than the Euclidean case (standard design) at its lower operating frequency (25 dB at 0.6 MHz compared to 23 dB at 2.2 MHz for the Euclidean case). Although the bandwidth around this peak sensitivity is smaller than that of the Euclidean case. It can been seen, unusually, that the $SG(3)$ device has a very flat response from 3 MHz upwards at a sensitivity level of 14 dB albeit at a much reduced decibel level from the main peak.

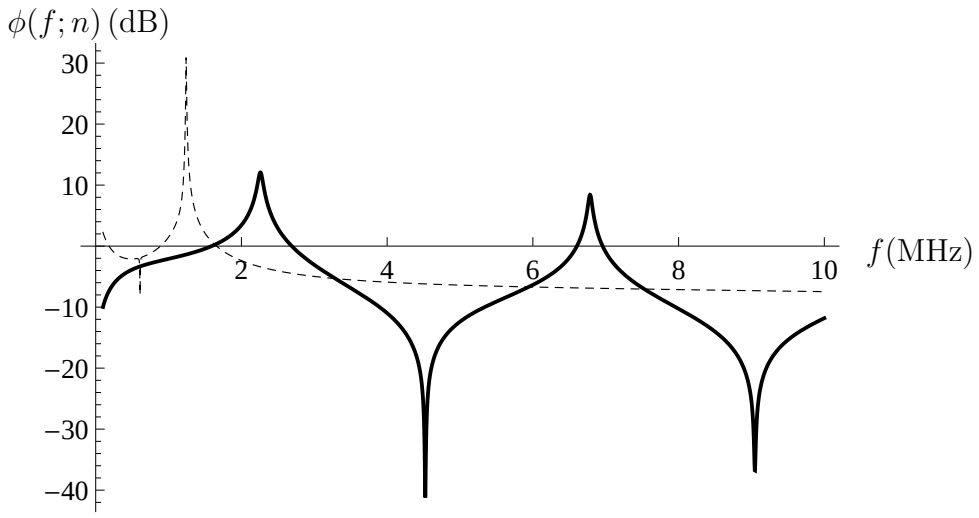

Figure 12: Non-dimensionalised reception sensitivity (equation (184)) versus frequency for the $SG(3)$ lattice transducer at fractal generation level $n = 1$ (dashed line). The non-dimensionalised reception sensitivity of the standard (Euclidean) transducer (equation (185)) is plotted for comparison (full line). Parameter values are given in Table 5.

With regard to the reception sensitivity the fractal design does show same encouraging results with a much higher peak amplitude than that of the Euclidean case and at a lower operating frequency (at 1.2 MHz its sensitivity is 31 dB whereas the peak sensitivity of the standard device is 12 dB at 2.2 MHz). Following this is an examination of next generation level ($n = 2$).

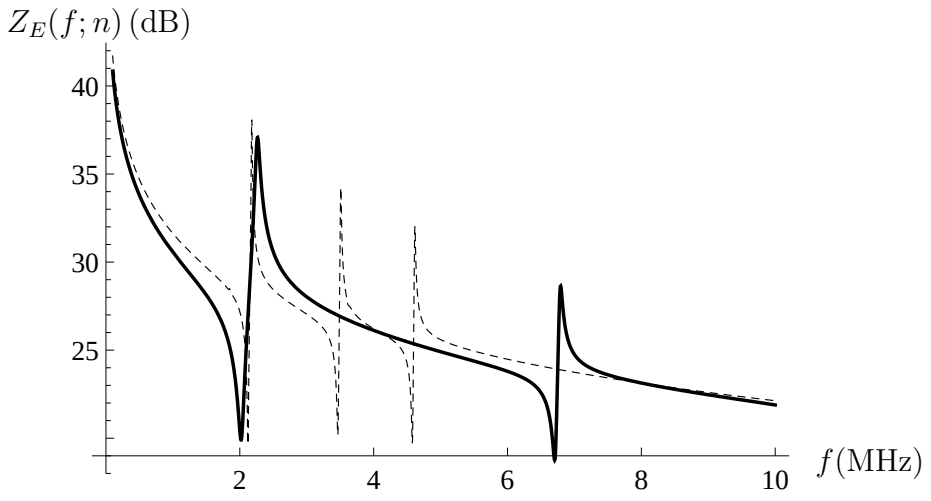

Figure 13: Non-dimensionalised electrical impedance (equation (154)) versus frequency for the $SG(3)$ lattice transducer at fractal generation level $n = 2$ (dashed line). The non-dimensionalised electrical impedance of the standard (Euclidean) transducer (equation (155)) is plotted for comparison (full line). Parameter values are given in Table 5.

The electrical impedance profile of the fractal design and the standard design follow a similar profile with more resonances being present in the fractal case due to the presence of a range of length scales in the new design. Indeed, for all the results that we will show, the resonant modes occur at higher frequencies as the generation level increases (that is, as the length scale of the lattice edges decreases).

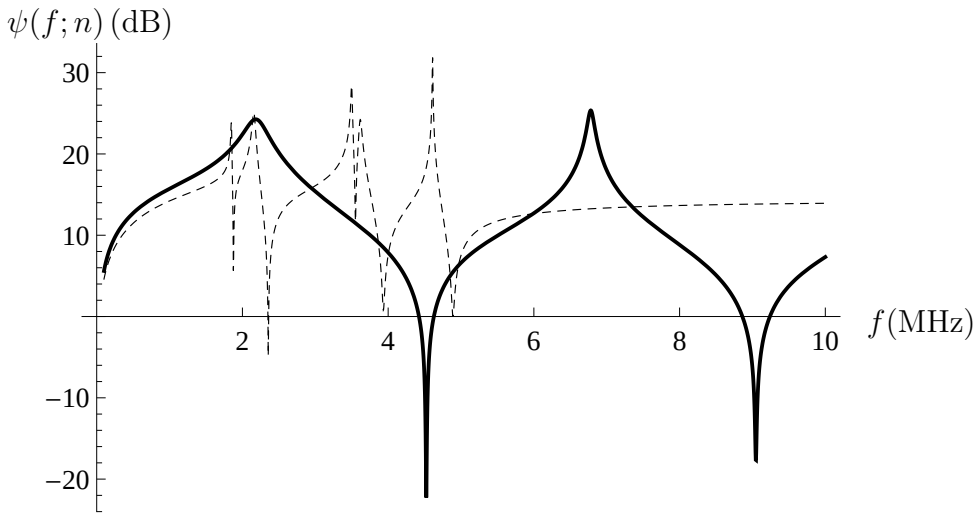

Figure 14: Non-dimensionalised transmission sensitivity (equation (170)) versus frequency for the $SG(3)$ lattice transducer at fractal generation level $n = 2$ (dashed line). The non-dimensionalised transmission sensitivity of the standard (Euclidean) transducer (equation (171)) is plotted for comparison (full line). Parameter values are given in Table 5.

In terms of the transmission sensitivity the maximum amplitude is somewhat higher in the fractal design than the Euclidean case (32 dB at 4.6 MHz compared to 24.7 dB at 2.2 MHz for the Euclidean case). Once again the bandwidth around this peak sensitivity is smaller than that of the Euclidean case.

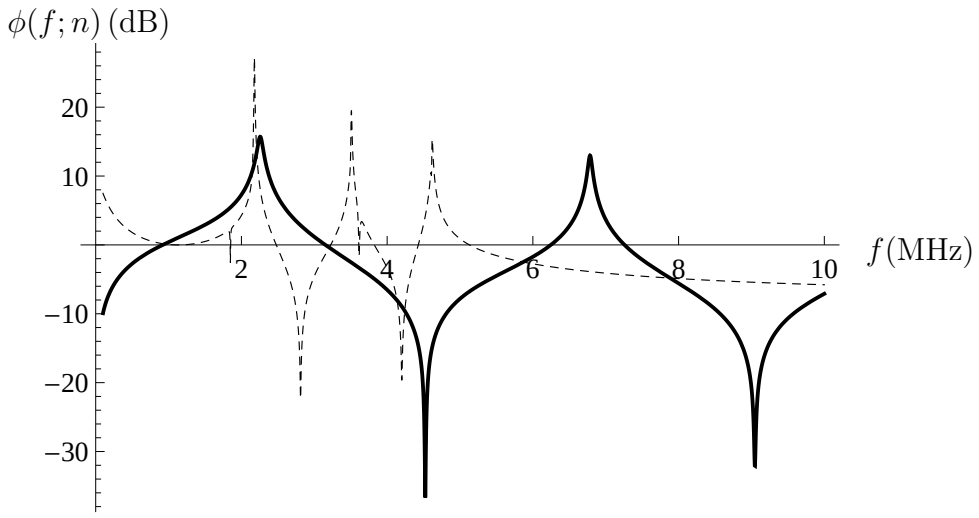

Figure 15: Non-dimensionalised reception sensitivity (equation (184)) versus frequency for the $SG(3)$ lattice transducer at fractal generation level $n = 2$ (dashed line). The non-dimensionalised reception sensitivity of the standard (Euclidean) transducer (equation (185)) is plotted for comparison (full line). Parameter values are given in Table 5.

The reception sensitivity has again a much higher peak amplitude than that of the Euclidean case at its lower operating frequency (at 2.2 MHz its sensitivity is 27 dB whereas the Peak sensitivity of the standard (Euclidean) device is 15.5 dB at 2.3 MHz). This examination can continue and below we consider the third generation level ($n = 3$) performance.

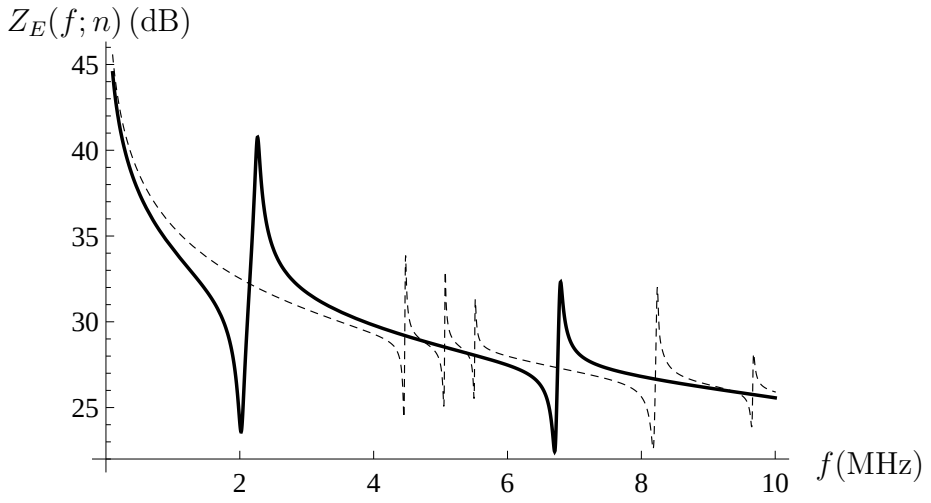

Figure 16: Non-dimensionalised electrical impedance (equation (154)) versus frequency for the $SG(3)$ lattice transducer at fractal generation level $n = 3$ (dashed line). The non-dimensionalised electrical impedance of the standard (Euclidean) transducer (equation (155)) is plotted for comparison (full line). Parameter values are given in Table 5.

As the generation level increases a grater range of length scales exist within the fractal design and so on increasing number of resonant modes emerge.

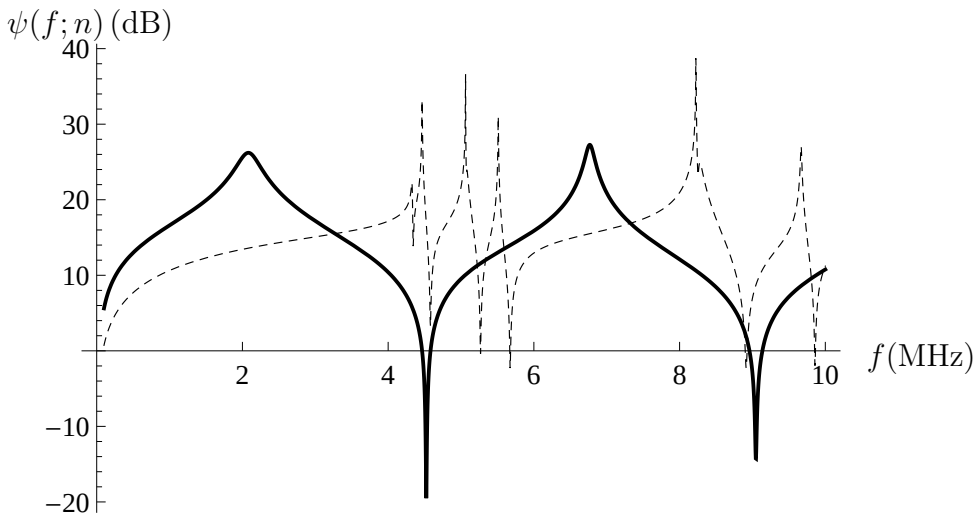

Figure 17: Non-dimensionalised transmission sensitivity (equation (170)) versus frequency for the $SG(3)$ lattice transducer at fractal generation level $n = 3$ (dashed line). The non-dimensionalised transmission sensitivity of the standard (Euclidean) transducer (equation (171)) is plotted for comparison (full line). Parameter values are given in Table 5.

As before the transmission sensitivity maximum amplitude is higher than the Euclidean case (39.7 dB at 8.2 MHz compared to 27.3 dB at 6.7 MHz for the Euclidean case), wih the bandwidth around this peak sensitivity being smaller than that of the Euclidean case.

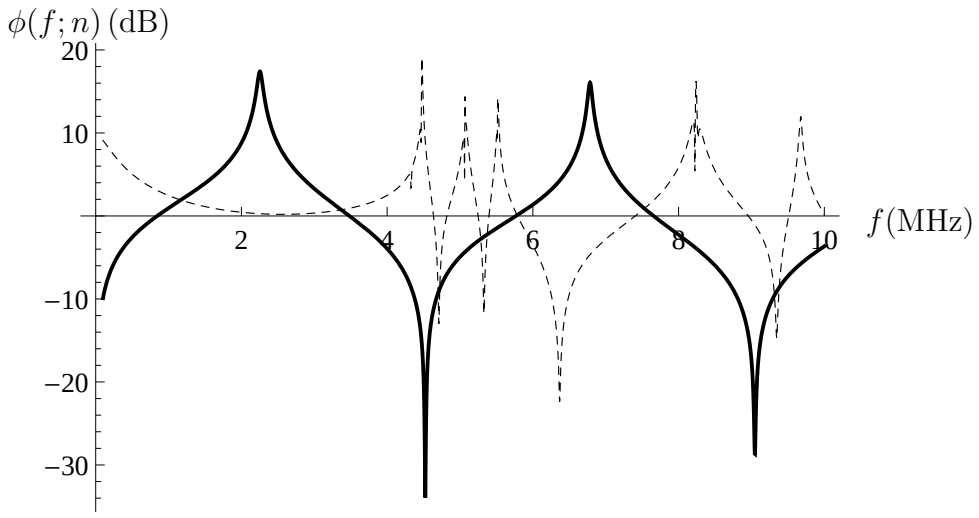

Figure 18: Non-dimensionalised reception sensitivity (equation (184)) versus frequency for the $SG(3)$ lattice transducer at fractal generation level $n = 3$ (dashed line). The non-dimensionalised reception sensitivity of the standard (Euclidean) transducer (equation (185)) is plotted for comparison (full line). Parameter values are given in Table 5.

The reception sensitivity is now more closely matched to the standard design in terms of peak amplitude (at 4.5 MHz its sensitivity is 19.3 dB and the peak sensitivity of the standard (Euclidean) device is 17.8 dB at 2.3 MHz).

8.2 Convergence

The norm of the difference between the energy in the power spectrum at successive generation levels, integrated with respect to frequency, is calculated for the transmission/reception sensitivities, as follows

$$\sum_{i=1}^{m} |\psi(f_i; n) - \psi(f_i; n+1)| = \psi^*(n), \tag{213}$$

and

$$\sum_{i=1}^{m} |\phi(f_i; n) - \phi(f_i; n+1)| = \phi^*(n). \tag{214}$$

where $\psi^*(n)$ and $\phi^*(n)$ record the convergence of the transmission and reception sensitivities respectively as the fractal generation level increases. Figures 19 and 20 shows the dependence of these norms on the generation level.

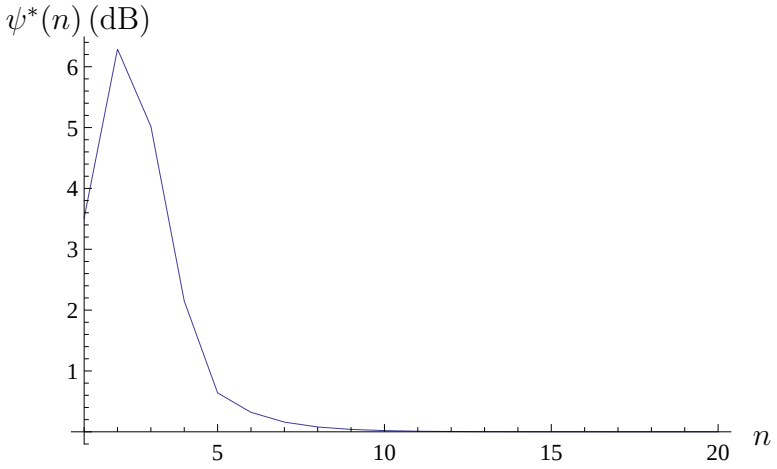

Figure 19: Non-dimensionalised transmission sensitivity ($\psi^*(n)$) (equation (213)) converges as the fractal generation level increases. This sensitivity converges by generation level $n = 10$ over this frequency range where $f_i \in [0.1, 10]$MHz.

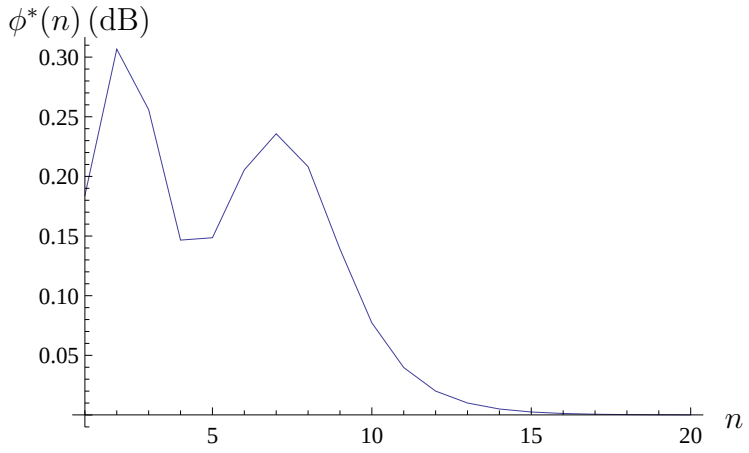

Figure 20: Non-dimensionalised reception sensitivity ($\phi^*(n)$) (equation (214)) versus successive generation levels. This sensitivity converges by generation level $n = 16$ over this frequency range where $f_i \in [0.1, 10]$MHz.

9 Conclusions

A model of a piezoelectric ultrasound transducer with a fractal geometry has been constructed and its operational qualities compared with that of a standard (Euclidean) design. The fractal that was used to simulate this self-similar transducer was the Sierpinski gasket [7]. The lattice counterpart of the Sierpinski gasket SG(3) [20] was used to express the electrical and mechanical fields in terms of a finite element methodology [14]. As this was the first time that a finite element analysis has been performed on this structure then some new basis functions were derived. The fractal design has multiple length scales (the standard design typically has a single length scale) and, since these are resonating devices, this resulted in a rich set of resonating frequencies. Indeed the broadband resonators found in nature and in musical instruments rely on this

principle. The finite element formulation resulted in a matrix equation whose solution yielded to a renormalisation approach. This is turn led to a small set of recursion relationships for the pivotal Green's functions that drive the calculation of the transmission/reception sensitivities of the device. The focus was on low generation levels of the fractal as these are most likely to adhere to manufacturing constraints. The results showed that the fractal transducer resonates at many more frequencies than the standard (Euclidean) transducer. Importantly, the fractal transducer gave rise to a significantly higher amplitude transmission and reception sensitivity than the standard (Euclidean) design. The convergence of the fractal device's performance as the fractal generation level increases was also considered. It was seen that, in both transmission and reception modes, the outputs converge by generation levels $n = 10$ and $n = 16$ respectively. These encouraging results suggest that it will be worthwhile studying other fractal designs. A program to manufacture these fractal transducers has been instigated and the comparison between the theoretical and experimental results will be the subject of a future investigation.

10 Appendix

		Adjacent vertices to (x_j, y_j)		
j	(x_j, y_j)	(x_{j+1}, y_{j+1})	(x_{j+2}, y_{j+2})	(x_{j+3}, y_{j+3})
1	$(0, 0)$	A	2	3
2	$(h, 0)$	1	3	B
3	$(\frac{h}{2}, \frac{\sqrt{3}}{2}h)$	1	2	C
A	$(-h, 0)$	1		
B	$(2h, 0)$	2		
C	$(h, \sqrt{3}h)$	5		

Table 1: Coordinates of the vertices and a list of the adjacent vertices to vertex (x_j, y_j) for generation level $n = 1$. The vertex labelling is given in Figure 5.

		Adjacent vertices to (x_j, y_j)		
j	(x_j, y_j)	(x_{j+1}, y_{j+1})	(x_{j+2}, y_{j+2})	(x_{j+3}, y_{j+3})
1	$(0, 0)$	A	2	3
2	$(h, 0)$	1	3	4
3	$(\frac{h}{2}, \frac{\sqrt{3}}{2}h)$	1	2	7
4	$(2h, 0)$	2	5	6
5	$(3h, 0)$	B	4	6
6	$(\frac{5h}{2}, \frac{\sqrt{3}}{2}h)$	4	5	8
7	$(h, \sqrt{3}h)$	3	8	9
8	$(2h, \sqrt{3}h)$	6	7	9
9	$(\frac{3h}{2}, \frac{3\sqrt{3}}{2}h)$	C	7	8
A	$(-h, 0)$	1		
B	$(4h, 0)$	5		
C	$(2h, 2\sqrt{3}h)$	9		

Table 2: Coordinates of the vertices and a list of the adjacent vertices to vertex (x_j, y_j) for generation level $n = 2$. The vertex labelling is given in Figure 6.

j	a	b	c	d
1	1	0	0	$-\frac{1}{h^2}$
2	0	$\frac{2}{h}$	0	$-\frac{1}{h^2}$
3	0	$\frac{1}{h}$	$\frac{\sqrt{3}}{h}$	$-\frac{1}{h^2}$
A	0			$\frac{1}{h^2}$
B	$-\frac{1}{3}$			$\frac{1}{3h^2}$
C	$-\frac{1}{3}$			$\frac{1}{3h^2}$

Table 3: Coefficients of the basis functions ϕ_j for generation level $n = 1$.

j	a	b	c	d
1	1	0	0	$-\frac{1}{h^2}$
2	0	$\frac{2}{h}$	0	$-\frac{1}{h^2}$
3	0	$\frac{1}{h}$	$\frac{\sqrt{3}}{h}$	$-\frac{1}{h^2}$
4	-3	$\frac{4}{h}$	0	$-\frac{1}{h^2}$
5	-8	$\frac{6}{h}$	0	$-\frac{1}{h^2}$
6	-6	$\frac{5}{h}$	$\frac{\sqrt{3}}{h}$	$-\frac{1}{h^2}$
7	-3	$\frac{7}{h}$	$\frac{2\sqrt{3}}{h}$	$-\frac{1}{h^2}$
8	-6	$\frac{4}{h}$	$\frac{2\sqrt{3}}{h}$	$-\frac{1}{h^2}$
9	-8	$\frac{3}{h}$	$\frac{3\sqrt{3}}{h}$	$-\frac{1}{h^2}$
A	0			$\frac{1}{h^2}$
B	$-\frac{9}{7}$			$\frac{1}{7h^2}$
C	$-\frac{9}{7}$			$\frac{1}{7h^2}$

Table 4: Coefficients of the basis functions ϕ_j for generation level $n = 2$.

Design Parameter	Symbol	Magnitude	Dimensions
Parallel electrical load	Z_q	1000	Ohms
Series electrical load	Z_0	50	Ohms
Mechanical impedance of backing layer	Z_B	0.022	MRayls
Mechanical impedance of load	Z_L	1.5	MRayls
Length of fractal	L	1	mm
The wave speed of the load Mechanical impedance	c_L	1500	N/m^2
Density of the load Mechanical impedance	ρ_L	1000	kgm^{-3}
Density of the transducer Mechanical impedance	ρ_T	7500	kgm^{-3}

Table 5: Parameter Values for the Sierpinski Gasket Transducer.

The material properties of PZT-5H are [3]

$$c_{pq} = \begin{bmatrix} 12.6 & 7.95 & 8.41 & 0 & 0 & 0 \\ 7.95 & 12.6 & 8.41 & 0 & 0 & 0 \\ 8.41 & 8.41 & 11.7 & 0 & 0 & 0 \\ 0 & 0 & 0 & 2.3 & 0 & 0 \\ 0 & 0 & 0 & 0 & 2.3 & 0 \\ 0 & 0 & 0 & 0 & 0 & 2.325 \end{bmatrix} \times 10^{10} N/m^2, \tag{215}$$

$$e_{ip} = \begin{bmatrix} 0 & 0 & 0 & 0 & 17 & 0 \\ 0 & 0 & 0 & 17 & 0 & 0 \\ -6.5 & -6.5 & 23.3 & 0 & 0 & 0 \end{bmatrix} C/m^2, \tag{216}$$

$$\varepsilon_{ij} = \begin{bmatrix} 1700\varepsilon_0 & 0 & 0 \\ 0 & 1700\varepsilon_0 & 0 \\ 0 & 0 & 1470\varepsilon_0 \end{bmatrix} C/(Vm). \tag{217}$$

where $\varepsilon_0 = 8.854 \times 10^{-12}\ C/(Vm)$.

References

[1] J. Abdulbake, A. J. Mulholland, and J. Gomatam. A renormalization approach to reaction-diffusion processes on fractals. *Fractas*, 11(4):315–330, (2003).

[2] J. Abdulbake, A. J. Mulholland, and J. Gomatam. Existence and stability of reaction-diffusion waves on a fractal lattice. *Chaos, Solitons and Fractas*, 20(4):799–814, (2004).

[3] B. A. Auld. *Acoustic Fields and Waves in Solids*, volume 1. John Wiley and Sons, New York, (1973).

[4] A. M. Chiselev, L. Moraru, and A. Gogu. Localization of an object using a bat model inspired from biology, romanian. *J. Biophys*, 19(4):251258, (2009).

[5] F. M. de Espinosa, O. Martinez, L. E. Segura, and L. Gomez-Ullate. Double frequency piezoelectric transducer design for harmonic imaging purposes in ndt. *IEEE T. Ultrason. Ferr*, 52(6):980986, (2005).

[6] D. F. Eberl, R. W. Hardy, and M. J. Kernan. Genetically similar transduction mechanisms for touch and hearing in drosophila. *J. Neurosci*, 20(16):59815988, (2000).

[7] K. Falconer. *Fractal Geometry: Mathematical Foundations and Applications*. John Wiley and Sons Ltd, Chichester, England, (2003).

[8] K. Falconer and J. Hu. Nonlinear diffusion equations on unbounded fractal domains. *J Math Anal App*, 256:606–624, (2001).

[9] G. Hayward. A systems feedback representation of piezoelectric transducer operational impedance. *Ultrasonics*, 22:153–162, (1984).

[10] G. Hayward, C. J. MacLeod, and T. S. Durrani. A systems model of the thickness mode piezoelectric transducer. *J. Acoust. Soc. Am*, 76(2):369–382, (1984).

[11] J. Kigami. *Analysis on Fractals*. Cambridge University Press, Cambridge, UK, (2001).

[12] Giona M. Transport phenomena in fractal and heterogeneous media: Input/output renormalization and exact results. *Chaos, Solitons and Fractas*, 7(9):1371–1396, (1996).

[13] R. N. Miles and R. R. Hoy. The development of a biologically-inspired directional microphone for hearing aids. *Audiol Neurootol*, 11(2):86–94, (2006).

[14] A. J. Mulholland. Bounds on the Hausdorff dimension of a renormalisation map arising from an excitable reaction-diffusion system on a fractal lattice. *Chaos, Solitons and Fractals*, 35(2):274–284, (2008).

[15] R. Mller. A numerical study of the role of the tragus in the big brown bat. *J. Acoust. Soc. Am*, 116(6):37013712, (2004).

[16] R. Mller, H. Lu, S. Zhang, and H. Peremans. A helical biosonar scanning pattern in the chinese noctule nycatalus plancyi. *J. Acoust. Soc. Am*, 119(6):40834092, (2006).

[17] B. Nadrowski, J. T. Albert, and M. C. Gpfert. Transducer-based force generation explains active process in drosophilia hearing. *Curr. Biol*, 18:13651372, (2008).

[18] L. A. Orr, A. J. Mulholland, R. L. O'Leary, A. Parr, R. Pethrick, and G. Hayward. Theoretical modelling of frequency dependent elastic loss in composite piezoelectric transducers. *Ultrasonics*, 47:130–137, (2007).

[19] D. Robert and M. C. Gpfert. Novel schemes for hearing and orientation in insects. *Curr. Opin. Neurobiol*, 12:715720, (2002).

[20] W. A. Schwalm and M. K. Schwalm. Extension theory for lattice Green functions. Phys.Rev.B. 37(16):9524–9542, (1988).

[21] J. Yang. *The Mechanics of Piezoelectric Structures*. World Scientific, Singapore, (2006).